Particulate Organic Matter Distributions in the Water Column of the Chukchi Sea during Late Summer

Miguel A Goni[1], Lauren W. Juranek[1], Rachel E. Sipler[2], and Kylie A Welch[1]

[1]Oregon State University
[2]Memorial University of Newfoundland

November 22, 2022

Abstract

Two oceanographic cruises were completed in September 2016 and August 2017 to investigate the distribution of particulate organic matter (POM) across the northeast Chukchi Shelf. Both periods were characterized by highly stratified conditions, with major contrasts in the distribution of regional water masses that impacted POM distributions. Overall, surface waters were characterized by low chlorophyll fluorescence (Chl Fl<0.8 mg m^{-3}) and particle beam attenuation (c_p<0.3 m^{-1}) values, and low concentrations of particulate organic carbon (POC<8 mmol m^{-3}), chlorophyll and pheophytin (Chl+Pheo<0.8 mg m^{-3}), and suspended particulate matter (SPM~2 g m^{-3}). Elevated Chl Fl and Chl+Pheo (~2 mg m^{-3}) values measured at mid-depths below the pycnocline defined the subsurface chlorophyll maxima (SCM), which exhibited moderate POC (~10 mmol m^{-3}), c_p (~0.4 m^{-1}) and SPM (~3 g m^{-3}). In contrast, deeper waters below the pycnocline were characterized by low Chl Fl and Chl+Pheo (~0.7 mg m^{-3}), high c_p (>1.5 m^{-1}) and SPM (>8 g m^{-3}) and elevated POC (>10 mmol m^{-3}). POM compositions from surface and SCM regions of the water column were consistent with contributions from active phytoplankton sources whereas samples from bottom waters were characterized by high Pheo/(Chl+Pheo) ratios (>0.4) indicative of altered phytoplankton detritus. Marked contrasts in POM were observed in both surface and mid-depth waters during both cruises. Increases in chlorophyll and POC were measured in mid-depth waters during the September 2016 cruise following a period of downwelling-favorable winds, and in surface waters during the August 2017 cruise following a period of upwelling-favorable winds.

Particulate Organic Matter Distributions in the Water Column of the Chukchi Sea during Late Summer

Miguel A. Goñi[1], Lauren W. Juranek[1], Rachel E. Sipler[2]+, Kylie A. Welch[1]

[1]College of Earth, Ocean, and Atmospheric Sciences, Oregon State University, Corvallis, OR 97331.

[2]Memorial University of Newfoundland, St. John's, NL Canada

[3]Affiliation for author 3.

Corresponding author: Miguel Goni1 (*miguel.goni@oregonstate.edu)*

+Current Address: Bigelow Laboratory for Ocean Sciences, East Boothbay, ME 04544.

Table 1. Summary of bottle data from samples collected at different depths along CTD transects during SKQ201612S and SKQ201712S cruises.

Sample Water Depth	Temperature (°C)	Salinity	Density (σ_t; kg m^{-3})	Density (σ_t; kg m^{-3})	Chl Fl (mg m^{-3})	Chl Fl (mg m^{-3})	c_p (m^{-1})	c_p (m^{-1})	POC (mmol m^{-3})	POC (mmol m^{-3})	Chl+Pheo (mg m^{-3})	Chl+Pheo (mg m^{-3})	SPM (g m^{-3})

SKQ2016 Cruise Transects (Sep 12-23, 2016)	**SKQ2016 Cruise Transects (Sep 12-23, 2016)**	**SKQ2016 Cruise Transects (Sep 12-23, 2016)**	**SKQ2016 Cruise Transects (Sep 12-23, 2016)**										
Surface													
Avg. +/- St.Dev.	0.72±1.43	28.12±0.67	22.51±0.48	22.51±0.48	0.59±0.21	0.59±0.21	0.21±0.09	0.21±0.09	7.22±3.32	7.22±3.32	0.69±1.76	0.69±1.76	2.30±
Min / Max	-1.25/4.09	27.21/30.21	21.82/23.92	21.82/23.92	0.21/1.15	0.21/1.15	0.06/0.68	0.06/0.68	2.76/19.86	2.76/19.86	0.21/9.82	0.21/9.82	0.65/
Median	0.50	27.88	22.36	22.36	0.56	0.56	0.20	0.20	6.35	6.35	0.37	0.37	2.19
Mid-Depth													
Avg. +/- St.Dev.	0.69±1.67	31.15±0.93	24.95±0.76	24.95±0.76	1.65±1.44	1.65±1.44	0.26±0.22	0.26±0.22	7.62±4.98	7.62±4.98	1.34±2.37	1.34±2.37	2.76±
Min / Max	-1.42/4.98	27.82/32.20	20.32/25.87	20.32/25.87	0.18/9.20	0.18/9.20	0.06/1.35	0.06/1.35	3.12/34.56	3.12/34.56	0.32/13.26	0.32/13.26	0.44/
Median	0.45	31.36	25.18	25.18	1.22	1.22	0.20	0.20	6.38	6.38	0.71	0.71	2.36
Bottom													
Avg. +/- St.Dev.	-0.14±0.57	32.26±0.09	25.90±0.08	25.90±0.08	0.55±0.19	0.55±0.19	1.64±0.49	1.64±0.49	9.89±2.09	9.89±2.09	0.72±0.12	0.72±0.12	7.65±
Min / Max	-1.53/1.38	32.05/32.45	25.74/26.12	25.74/26.12	0.12/1.14	0.12/1.14	0.80/3.07	0.80/3.07	5.35/14.12	5.35/14.12	0.52/0.82	0.52/0.82	3.37/
Median	-0.06	32.28	25.90	25.90	0.55	0.55	1.60	1.60	10.03	10.03	0.74	0.74	7.15
SKQ2017 Cruise Transects (Aug 10-20, 2017)	**SKQ2017 Cruise Transects (Aug 10-20, 2017)**	**SKQ2017 Cruise Transects (Aug 10-20, 2017)**	**SKQ2017 Cruise Transects (Aug 10-20, 2017)**										
Surface													
Avg. +/- St.Dev.	5.24±1.41	30.60±0.87	24.15±0.64	24.15±0.64	0.44±0.56	0.44±0.56	0.30±0.29	0.30±0.29	7.60±6.07	7.60±6.07	0.78±0.51	0.78±0.51	2.67±
Min / Max	2.06/8.23	28.41/33.12	22.47/26.52	22.47/26.52	0.00/3.32	0.00/3.32	0.11/1.76	0.11/1.76	0.60/31.65	0.60/31.65	0.23/1.52	0.23/1.52	0.24/
Median	4.96	30.88	24.27	24.27	0.25	0.25	0.18	0.18	5.70	5.70	0.54	0.54	2.39

Mid-Depth													
Avg. +/- St.Dev.	2.02±2.63	31.72±0.36	25.30±0.39	25.30±0.39	2.73±2.66	2.73±2.66	0.57±0.50	0.57±0.50	10.71±6.88	10.71±6.88	1.97±0.88	1.97±0.88	4.15±
Min / Max	-1.61/7.78	30.29/32.34	24.04/25.87	24.04/25.87	0.14/15.04	0.14/15.04	0.09/2.74	0.09/2.74	0.38/39.37	0.38/39.37	0.19/3.83	0.19/3.83	0.81/
Median	0.97	31.79	25.41	25.41	1.71	1.71	0.39	0.39	9.49	9.49	2.03	2.03	3.45
Bottom													
Avg. +/- St.Dev.	1.05±1.94	32.28±0.62	25.83±0.54	25.83±0.54	0.89±1.07	0.89±1.07	1.72±0.91	1.72±0.91	11.50±8.10	11.50±8.10	0.75±0.34	0.75±0.34	8.19±
Min /Max	-1.60/7.64	31.01/34.58	24.61/27.75	24.61/27.75	0.09/7.80	0.09/7.80	0.43/7.38	0.43/7.38	0.25/69.14	0.25/69.14	0.16/1.59	0.16/1.59	1.95/
Median	0.38	32.17	25.80	25.80	0.52	0.52	1.58	1.58	10.08	10.08	0.68	0.68	7.56

Captions: Avg., average; St.Dev., standard deviation; Min, minimum; Max, maximum; Chl Fl, chlorophyll fluorescence; c_p, particle beam attenuation; POC, particulate organic carbon; Chl+Pheo, combined pigments chlorophyll and pheophytin; SPM, suspended particulate matter.

Table 2. Compositions (Average ± standard deviation) of density-binned Niskin bottle samples from different water masses during SKQ201612S.

Density Bins σ_t (kg m-3)	Chl Fl (mg m^{-3})	Chl Fl (mg m^{-3})	c_p. (m^{-1})	c_p. (m^{-1})	POC (mmol m^{-3})	POC (mmol m^{-3})	Chl+Pheo (mg m^{-3})	Chl+Pheo (mg m^{-3})	SP (g
Transects 2, 3, 4, 5 (Sep 12-17, 2016)	**Transects 2, 3, 4, 5 (Sep 12-17, 2016)**	**Transects 2, 3, 4, 5 (Sep 12-17, 2016)**	**Transects 2, 3, 4, 5 (Sep 12-17, 2016)**						
Melt Water (MW)	Melt Water (MW)	Melt Water (MW)							
21.0 - 23.0	0.54 ± 0.19	0.54 ± 0.19	0.21 ± 0.10	0.21 ± 0.10	7.77 ± 2.65	7.77 ± 2.65	0.37 ± 0.09	0.37 ± 0.09	1.8 0.4
23.0 -24.0	1.04 ± 0.55	1.04 ± 0.55	0.21 ± 0.01	0.21 ± 0.01	6.18 ± 0.84	6.18 ± 0.84	0.50 ± 0.25	0.50 ± 0.25	2.1 0.2
Alaska Coastal Water (ACW)	Alaska Coastal Water (ACW)	Alaska Coastal Water (ACW)							
24.0 - 25.0	n.m.	n.m.	n.m.	n.m.	n.m.	n.m.	n.m.	n.m.	n.r
Bering-Chukchi Summer Water (BCSW)	Bering-Chukchi Summer Water (BCSW)	Bering-Chukchi Summer Water (BCSW)	Bering-Chukchi Summer Water (BCSW)	Bering-Chukchi Summer Water (BCSW)					

23.5 - 24.0	n.m.	n.m.	n.m.	n.m.	n.m.	n.m.	n.m.	n.m.	n.r
24.0 - 25.5	1.52 $\pm$ 0.49	1.52 $\pm$ 0.49	0.24 $\pm$ 0.04	0.24 $\pm$ 0.04	7.19 $\pm$ 2.14	7.19 $\pm$ 2.14	0.65 $\pm$ 0.22	0.65 $\pm$ 0.22	1.9 0.2
25.5 - 27.0	1.04 $\pm$ 1.05	1.04 $\pm$ 1.05	1.28 $\pm$ 0.56	1.28 $\pm$ 0.56	9.23 $\pm$ 2.68	9.23 $\pm$ 2.68	1.20 $\pm$ 0.56	1.20 $\pm$ 0.56	6.0 2.4
Bering-Chukchi Winter Water (BCWW)	Bering-Chukchi Winter Water (BCWW)	Bering-Chukchi Winter Water (BCWW)	Bering-Chukchi Winter Water (BCWW)	Bering-Chukchi Winter Water (BCWW)					
24.0 - 25.5	1.45 $\pm$ 1.04	1.45 $\pm$ 1.04	0.16 $\pm$ 0.07	0.16 $\pm$ 0.07	6.76 $\pm$ 1.54	6.76 $\pm$ 1.54	0.87 $\pm$ 0.58	0.87 $\pm$ 0.58	2.3 0.3
25.5 - 27.0	0.65 $\pm$ 0.53	0.65 $\pm$ 0.53	1.46 $\pm$ 0.59	1.46 $\pm$ 0.59	10.0 $\pm$ 2.79	10.0 $\pm$ 2.79	0.87 $\pm$ 0.51	0.87 $\pm$ 0.51	5.8 2.5
Atlantic Water (AtlW)	Atlantic Water (AtlW)	Atlantic Water (AtlW)							
27.0 - 28.0	n.m.	n.m.	n.m.	n.m.	n.m.	n.m.	n.m.	n.m.	n.r
Transects 6, 7, 8 (Sep 20-23, 2016)	**Transects 6, 7, 8 (Sep 20-23, 2016)**	**Transects 6, 7, 8 (Sep 20-23, 2016)**							
Melt Water (MW)	Melt Water (MW)	Melt Water (MW)							
21.0 -23.0	0.70 $\pm$ 0.23	0.70 $\pm$ 0.23	0.25 $\pm$ 0.06	0.25 $\pm$ 0.06	8.37 $\pm$ 4.43	8.37 $\pm$ 4.43	n.m.	n.m.	2.8 0.8
23.0 - 24.0	0.45 $\pm$ 0.16	0.45 $\pm$ 0.16	0.11 $\pm$ 0.04	0.11 $\pm$ 0.04	4.14 $\pm$ 0.84	4.14 $\pm$ 0.84	n.m.	n.m.	2.4 0.4
Alaska Coastal Water (ACW)	Alaska Coastal Water (ACW)	Alaska Coastal Water (ACW)							
24.0 - 25.0	n.m.	n.m.	n.m.	n.m.	n.m.	n.m.	n.m.	n.m.	n.r
Bering-Chukchi Sum-mer Water (BCSW)	Bering-Chukchi Sum-mer Water (BCSW)	Bering-Chukchi Sum-mer Water (BCSW)	Bering-Chukchi Sum-mer Water (BCSW)	Bering-Chukchi Sum-mer Water (BCSW)					
23.5 - 24.0	0.80 $\pm$ 0.25	0.80 $\pm$ 0.25	0.12 $\pm$ 0.01	0.12 $\pm$ 0.01	3.90 $\pm$ n.a.	3.90 $\pm$ n.a.	n.m.	n.m.	2.1 0.1
24.0 - 25.5	1.25 $\pm$ 0.75	1.25 $\pm$ 0.75	0.18 $\pm$ 0.10	0.18 $\pm$ 0.10	4.61 $\pm$ 1.66	4.61 $\pm$ 1.66	n.m.	n.m.	2.5 0.3
25.5 - 27.0	0.82 $\pm$ 0.80	0.82 $\pm$ 0.80	1.39 $\pm$ 0.60	1.39 $\pm$ 0.60	9.12 $\pm$ 2.02	9.12 $\pm$ 2.02	n.m.	n.m.	7.1 3.0

Bering-Chukchi Winter Water (BCWW)	Bering-Chukchi Winter Water (BCWW)	Bering-Chukchi Winter Water (BCWW)	Bering-Chukchi Winter Water (BCWW)	Bering-Chukchi Winter Water (BCWW)					
24.0 - 25.5	2.93 ± 2.87	2.93 ± 2.87	0.32 ± 0.21	0.32 ± 0.21	12.2 ± 11.8	12.2 ± 11.8	n.m.	n.m.	4.5 2.4
25.5 - 27.0	0.75 ± 0.71	0.75 ± 0.71	1.79 ± 0.68	1.79 ± 0.68	10.8 ± 1.76	10.8 ± 1.76	n.m.	n.m.	9.0 2.7
Atlantic Water (AtlW)	Atlantic Water (AtlW)	Atlantic Water (AtlW)							
26.0 - 27.0	n.m.	n.m.	n.m.	n.m.	n.m.	n.m.	n.m.	n.m.	n.r

Abbreviations: Chl Fl, chlorophyll concentration based on fluorescence; c_p, particle beam attenuation; POC, particulate organic carbon concentration; Chl+Pheo, chlorophyll plus pheophytin concentrations, SPM, suspended particulate matter.

Table 3. Compositions (Average ± standard deviation) of density-binned Niskin bottle samples from different water masses during SKQ201712S.

Density Bins σ_t (kg m-3)	Chl Fl (mg m^{-3})	Chl Fl (mg m^{-3})	c_p. (m^{-1})	c_p. (m^{-1})	POC (mmol m^{-3})	POC (mmol m^{-3})	Chl+Pheo (mg m^{-3})	Chl+Pheo (mg m^{-3})	SP (g
Transects 1, 2, 3, 4 (Aug 10-16, 2017)	**Transects 1, 2, 3, 4 (Aug 10-16, 2017)**	**Transects 1, 2, 3, 4 (Aug 10-16, 2017)**	**Transects 1, 2, 3, 4 (Aug 10-16, 2017)**						
Melt Water (MW)	Melt Water (MW)	Melt Water (MW)							
21.0 - 23.0	0.16 ± n.a.	0.16 ± n.a.	0.14 ± n.a.	0.14 ± n.a.	3.10 ± n.a.	3.10 ± n.a.	1.48 ± n.a.	1.48 ± n.a.	1.5 n.a
23.0 -24.0	0.09 ± 0.06	0.09 ± 0.06	0.15 ± 0.03	0.15 ± 0.03	4.79 ± 2.18	4.79 ± 2.18	0.23 ± n.a.	0.23 ± n.a.	2.0 0.7
Alaska Coastal Water (ACW)	Alaska Coastal Water (ACW)	Alaska Coastal Water (ACW)							
24.0 - 25.0	1.27 ± 0.53	1.27 ± 0.53	1.41 ± 0.45	1.41 ± 0.45	15.6 ± 2.84	15.6 ± 2.84	1.03 ± 0.47	1.03 ± 0.47	6.5 1.4
Bering-Chukchi Summer Water (BCSW)	Bering-Chukchi Summer Water (BCSW)	Bering-Chukchi Summer Water (BCSW)	Bering-Chukchi Summer Water (BCSW)	Bering-Chukchi Summer Water (BCSW)					
23.5 - 24.0	0.18 ± 0.13	0.18 ± 0.13	0.18 ± 0.02	0.18 ± 0.02	3.80 ± 1.98	3.80 ± 1.98	1.40 ± n.a.	1.40 ± n.a.	2.7 0.8

24.0 - 25.5	1.40 ± 2.20	1.40 ± 2.20	0.43 ± 0.54	0.43 ± 0.54	7.00 ± 3.94	7.00 ± 3.94	0.75 ± 0.67	0.75 ± 0.67	3.0 1.8
25.5 - 27.0	1.43 ± 1.87	1.43 ± 1.87	1.43 ± 0.95	1.43 ± 0.95	11.4 ± 5.99	11.4 ± 5.99	1.43 ± 0.92	1.43 ± 0.92	6.9 3.4
Bering-Chukchi Winter Water (BCWW)	Bering-Chukchi Winter Water (BCWW)	Bering-Chukchi Winter Water (BCWW)	Bering-Chukchi Winter Water (BCWW)	Bering-Chukchi Winter Water (BCWW)					
24.0 - 25.5	3.78 ± 2.60	3.78 ± 2.60	0.75 ± 0.70	0.75 ± 0.70	9.59 ± 3.71	9.59 ± 3.71	n.m.	n.m.	4.8 3.5
25.5 - 27.0	1.65 ± 1.94	1.65 ± 1.94	1.37 ± 0.78	1.37 ± 0.78	12.4 ± 6.82	12.4 ± 6.82	1.08 ± 0.68	1.08 ± 0.68	6.3 2.8
Atlantic Water (AtlW)	Atlantic Water (AtlW)	Atlantic Water (AtlW)							
27.0 - 28.0	n.m.	n.m.	n.m.	n.m.	n.m.	n.m.	n.m.	n.m.	n.n
Transects 5, 6, 7 (Aug 16-20, 2017)	**Transects 5, 6, 7 (Aug 16-20, 2017)**	**Transects 5, 6, 7 (Aug 16-20, 2017)**							
Melt Water (MW)	Melt Water (MW)	Melt Water (MW)							
21.0 -23.0	0.10 ± n.a.	0.10 ± n.a.	0.14 ± n.a.	0.14 ± n.a.	5.70 ± n.a.	5.70 ± n.a.	0.77 ± n.a.	0.77 ± n.a.	2.3 n.a
23.0 - 24.0	0.30 ± 0.42	0.30 ± 0.42	0.34 ± 0.34	0.34 ± 0.34	8.07 ± 4.72	8.07 ± 4.72	0.54 ± n.a.	0.54 ± n.a.	2.8 2.2
Alaska Coastal Water (ACW)	Alaska Coastal Water (ACW)	Alaska Coastal Water (ACW)							
24.0 - 25.0	1.61 ± 0.86	1.61 ± 0.86	0.63 ± 0.16	0.63 ± 0.16	18.0 ± 5.79	18.0 ± 5.79	1.59 ± 0.46	1.59 ± 0.46	3.3 1.1
Bering-Chukchi Summer Water (BCSW)	Bering-Chukchi Summer Water (BCSW)	Bering-Chukchi Summer Water (BCSW)	Bering-Chukchi Summer Water (BCSW)	Bering-Chukchi Summer Water (BCSW)					
23.5 - 24.0	0.33 ± 0.07	0.33 ± 0.07	0.19 ± 0.01	0.19 ± 0.01	4.56 ± 0.49	4.56 ± 0.49	n.m.	n.m.	2.2 1.1
24.0 - 25.5	1.16 ± 1.43	1.16 ± 1.43	0.50 ± 0.52	0.50 ± 0.52	8.95 ± 5.36	8.95 ± 5.36	2.11 ± 1.71	2.11 ± 1.71	3.7 2.2
25.5 - 27.0	1.92 ± 2.82	1.92 ± 2.82	1.54 ± 1.19	1.54 ± 1.19	12.0 ± 11.5	12.0 ± 11.5	1.23 ± 1.22	1.23 ± 1.22	8.1 4.4

Bering-Chukchi Winter Water (BCWW)	Bering-Chukchi Winter Water (BCWW)	Bering-Chukchi Winter Water (BCWW)	Bering-Chukchi Winter Water (BCWW)	Bering-Chukchi Winter Water (BCWW)					
24.0 - 25.5	0.44 ± 0.33	0.44 ± 0.33	0.12 ± 0.03	0.12 ± 0.03	3.98 ± 2.61	3.98 ± 2.61	n.m.	n.m.	2.6 0.6
25.5 - 27.0	1.98 ± 1.54	1.98 ± 1.54	1.19 ± 0.66	1.19 ± 0.66	10.7 ± 5.96	10.7 ± 5.96	0.68 ± n.a.	0.68 ± n.a.	5.8 2.3
Atlantic Water (AtlW)	Atlantic Water (AtlW)	Atlantic Water (AtlW)							
26.0 - 27.0	0.21 ± 0.08	0.21 ± 0.08	1.55 ± 0.67	1.55 ± 0.67	11.9 ± 4.09	11.9 ± 4.09	0.86 ± 0.20	0.86 ± 0.20	10. 4.9

Abbreviations: Chl Fl, chlorophyll concentration based on fluorescence; c_p, particle beam attenuation; POC, particulate organic carbon concentration; Chl+Pheo, chlorophyll plus pheophytin concentrations, SPM, suspended particulate matter.

Table 4. Particulate organic matter compositions of density-binned Niskin bottle samples from different water masses during SKQ201612S and SKQ21712S.

Water Mass Cruise Period	Density Bins σ_t (kg m^{-3})	Chl Fl:POC (mg g^{-1})	POC:c_p (mmol m^{-2})	POC:c_p (mmol m^{-2})	Pheo/ (Chl+Pheo)	Pheo/ (Chl+Pheo)	POC:SPM (mass %)	POC:SI (mass %)
Melt Water (MW)								
SKQ2016 Sep 12-17, 2016	21.0 - 23.0	6.3 ± 3.1	40.6 ± 24.1	40.6 ± 24.1	0.10 ± 0.06	0.10 ± 0.06	6.0 ± 2.6	6.0 ± 2.6
SKQ2016 Sep 20-23, 2016	21.0 - 23.0	8.1 ± 5.1	30.5 ± 18.0	30.5 ± 18.0	n.m.	n.m.	3.8 ± 2.3	3.8 ± 2.3
SKQ2017 Aug 10-16, 2017	21.0 - 23.0	4.3 ± n.a.	21.7 ± n.a.	21.7 ± n.a.	0.18 ± n.a.	0.18 ± n.a.	2.4 ± n.a.	2.4 ± n.a.
SKQ2017 Aug 16-20, 2017	21.0 - 23.0	1.4 ± n.a.	40.6 ± n.a.	40.6 ± n.a.	n.m.	n.m.	2.9 ± n.a.	2.9 ± n.a.
SKQ2016 Sep 12-17, 2016	23.0 - 24.0	13.8 ± 7.5	28.2 ± 4.2	28.2 ± 4.2	0.17 ± 0.20	0.17 ± 0.20	3.5 ± 0.6	3.5 ± 0.6

SKQ2016 Sep 20-23, 2016	23.0 - 24.0	9.5 ± 3.5	37.6 ± 12.4	37.6 ± 12.4	n.m.	n.m.	2.1 ± 0.5	2.1 ± 0.5
SKQ2017 Aug 10-16, 2017	23.0 - 24.0	1.9 ± 1.5	31.7 ± 16.0	31.7 ± 16.0	0.30 ± n.a.	0.30 ± n.a.	3.7 ± 2.2	3.7 ± 2.2
SKQ2017 Aug 16-20, 2017	23.0 - 24.0	2.2 ± 3.3	30.5 ± 35.7	30.5 ± 35.7	0.16 ± n.a.	0.16 ± n.a.	3.8 ± 3.7	3.8 ± 3.7
Alaska Coastal Water (ACW)	Alaska Coastal Water (ACW)							
SKQ2016 Sep 12-17, 2016	24.0 - 25.0	n.m.	n.m.	n.m.	n.m.	n.m.	n.m.	n.m.
SKQ2016 Sep 20-23, 2016	24.0 - 25.0	n.m.	n.m.	n.m.	n.m.	n.m.	n.m.	n.m.
SKQ2017 Aug 10-16, 2017	24.0 - 25.0	7.0 ± 3.2	11.7 ± 4.4	11.7 ± 4.4	0.22 ± 0.22	0.22 ± 0.22	2.9 ± 0.8	2.9 ± 0.8
SKQ2017 Aug 16-20, 2017	24.0 - 25.0	7.8 ± 4.8	29.4 ± 11.9	29.4 ± 11.9	0.06 ± 0.02	0.06 ± 0.02	7.2 ± 3.4	7.2 ± 3.4
Bering-Chukchi Summer Water (BCSW)	Bering-Chukchi Summer Water (BCSW)							
SKQ2016 Sep 12-17, 2016	23.5 - 24.0	n.m.	n.m.	n.m.	n.m.	n.m.	n.m.	n.m.
SKQ2016 Sep 20-23, 2016	23.5 - 24.0	22.3 ± n.a.	32.9 ± n.a.	32.9 ± n.a.	n.m.	n.m.	2.3 ± n.a.	2.3 ± n.a.
SKQ2017 Aug 10-16, 2017	23.5 - 24.0	3.6 ± 3.3	20.8 ± 12.6	20.8 ± 12.6	0.15 ± n.a.	0.15 ± n.a.	1.9 ± 1.2	1.9 ± 1.2

SKQ2017 Aug 16-20, 2017	23.5 - 24.0	6.0 ± 1.5	24.3 ± 2.8	24.3 ± 2.8	n.m.	n.m.	2.8 ± 1.5	2.8 ± 1.5
SKQ2016 Sep 12-17, 2016	24.0 - 25.5	18.8 ± 8.3	30.0 ± 10.5	30.0 ± 10.5	0.13 ± 0.05	0.13 ± 0.05	4.4 ± 1.5	4.4 ± 1.5
SKQ2016 Sep 20-23, 2016	24.0 - 25.5	21.7 ± 15.2	30.5 ± 21.0	30.5 ± 21.0	n.m.	n.m.	2.1 ± 0.8	2.1 ± 0.8
SKQ2017 Aug 10-16, 2017	24.0 - 25.5	13.9 ± 23.2	25.1 ± 34.7	25.1 ± 34.7	0.08 ± 0.09	0.08 ± 0.09	3.6 ± 3.0	3.6 ± 3.0
SKQ2017 Aug 16-20, 2017	24.0 - 25.5	10.1 ± 13.9	25.5 ± 30.6	25.5 ± 30.6	0.25 ± 0.44	0.25 ± 0.44	3.3 ± 2.8	3.3 ± 2.8
SKQ2016 Sep 12-17, 2016	25.5 - 27.0	10.0 ± 10.1	9.9 ± 1.6	9.9 ± 1.6	0.34 ± 0.0.16	0.34 ± 0.0.16	2.1 ± 0.3	2.1 ± 0.3
SKQ2016 Sep 20-23, 2016	25.5 - 27.0	8.0 ± 8.0	9.4 ± 4.6	9.4 ± 4.6	n.m.	n.m.	1.7 ± 0.8	1.7 ± 0.8
SKQ2017 Aug 10-16, 2017	25.5 - 27.0	11.2 ± 15.7	13.3 ± 11.3	13.3 ± 11.3	0.28 ± 0.29	0.28 ± 0.29	2.4 ± 1.7	2.4 ± 1.7
SKQ2017 Aug 16-20, 2017	25.5 - 27.0	15.3 ± 26.9	9.5 ± 11.7	9.5 ± 11.7	0.09 ± 0.14	0.09 ± 0.14	1.8 ± 2.0	1.8 ± 2.0
Table 3. continued.	**Table 3. continued.**							
Cruise Period	Density Bins σ_t (kg m^{-3})	Chl Fl:POC (mg g^{-1})	POC:c_p (mmol m^{-2})	POC:c_p (mmol m^{-2})	Pheo/ (Chl+Pheo)	Pheo/ (Chl+Pheo)	POC:SPM (mass %)	POC:SI (mass %
Bering-Chukchi Winter Water (BCWW)	Bering-Chukchi Winter Water (BCWW)							
SKQ2016 Sep 12-17, 2016	24.0 - 25.5	18.4 ± 14.0	43.7 ± 21.2	43.7 ± 21.2	0.20 ± 0.18	0.20 ± 0.18	3.4 ± 0.9	3.4 ± 0.9

SKQ2016 Sep 20-23, 2016	24.0 - 25.5	26.9 ± 37.0	28.0 ± 33.0	28.0 ± 33.0	n.m.	n.m.	2.7 ± 3.0	2.7 ± 3.0
SKQ2017 Aug 10-16, 2017	24.0 - 25.5	29.6 ± 23.3	21.8 ± 21.9	21.8 ± 21.9	n.m.	n.m.	3.0 ± 2.5	3.0 ± 2.5
SKQ2017 Aug 16-20, 2017	24.0 - 25.5	53.0 ± 52.6	36.3 ± 25.4	36.3 ± 25.4	n.m.	n.m.	1.9 ± 1.3	1.9 ± 1.3
SKQ2016 Sep 12-17, 2016	25.5 - 27.0	5.6 ± 4.8	8.0 ± 3.9	8.0 ± 3.9	0.41 ± 0.39	0.41 ± 0.39	2.5 ± 1.3	2.5 ± 1.3
SKQ2016 Sep 20-23, 2016	25.5 - 27.0	5.8 ± 5.6	8.7 ± 3.6	8.7 ± 3.6	n.m.	n.m.	1.6 ± 0.5	1.6 ± 0.5
SKQ2017 Aug 10-16, 2017	25.5 - 27.0	10.5 ± 13.6	12.8 ± 10.2	12.8 ± 10.2	0.30 ± 0.35	0.30 ± 0.35	2.7 ± 2.0	2.7 ± 2.0
SKQ2017 Aug 16-20, 2017	25.5 - 27.0	18.6 ± 17.8	13.6 ± 10.7	13.6 ± 10.7	0.26 ± n.a.	0.26 ± n.a.	2.7 ± 1.9	2.7 ± 1.9
Atlantic Water (AtlW)								
SKQ2016 Sep 12-17, 2016	27.0 - 28.0	n.m.	n.m.	n.m.	n.m.	n.m.	n.m.	n.m.
SKQ2016 Sep 20-23, 2016	27.0 - 28.0	n.m.	n.m.	n.m.	n.m.	n.m.	n.m.	n.m.
SKQ2017 Aug 10-16, 2017	27.0 - 28.0	n.m.	n.m.	n.m.	n.m.	n.m.	n.m.	n.m.
SKQ2017 Aug 16-20, 2017	27.0 - 28.0	1.4 ± 0.7	8.3 ± 4.5	8.3 ± 4.5	0.68 ± 0.21	0.68 ± 0.21	1.4 ± 0.8	1.4 ± 0.8

Compositions were determined by averaging the ratios of individual samples from the different density ranges and calculating their variability by applying propagation of error calculations to the standard deviations of the parameters ratioed. Abbreviations: Chl Fl:POC, chlorophyll fluorescence-particulate organic carbon ratio (mg g^{-1}); POC:c_p, particulate organic carbon-particle beam attenuation ratio (mmol m^{-2}); Pheo/(Chl+Pheo), pheophytin-combined chlorophyll plus pheophytin ratio (mg mg^{-1}); POC:SPM, particulate organic carbon-suspended particulate matter mass ratio (g g^{-1}) x 100 (%).

Hosted file

goni_etal_jgr_oceans_supp_figures.docx available at https://authorea.com/users/537664/articles/599398-particulate-organic-matter-distributions-in-the-water-column-of-the-chukchi-sea-during-late-summer

Hosted file

essoar.10507393.1.docx available at https://authorea.com/users/537664/articles/599398-particulate-organic-matter-distributions-in-the-water-column-of-the-chukchi-sea-during-late-summer

Miguel A. Goñi[1], Lauren W. Juranek[1], Rachel E. Sipler[2]†, Kylie A. Welch[1]

[1]College of Earth, Ocean, and Atmospheric Sciences, Oregon State University, Corvallis, OR 97331.

[2]Memorial University of Newfoundland, St. John's, NL Canada

[3]Affiliation for author 3.

Corresponding author: Miguel Goñi1 (miguel.goni@oregonstate.edu)

†Current Address: Bigelow Laboratory for Ocean Sciences, East Boothbay, ME 04544.

Key Points:

- There are marked contrasts in POM distributions and compositions associated with distinct water masses on the northeast Chukchi Shelf.
- Despite high stratification, wind events elicit increases of plankton-derived POM in sub-surface regions of the water column.
- Turbid bottom waters display elevated concentrations of mineral-rich particles enriched in altered POM likely resuspended from the seabed.

Abstract

Two oceanographic cruises were completed in September 2016 and August 2017 to investigate the distribution of particulate organic matter (POM) across the northeast Chukchi Shelf. Both periods were characterized by highly stratified conditions, with major contrasts in the distribution of regional water masses that impacted POM distributions. Overall, surface waters were characterized by low chlorophyll fluorescence (Chl Fl<0.8 mg m^{-3}) and particle beam attenuation (c_p<0.3 m^{-1}) values, and low concentrations of particulate organic carbon (POC<8 mmol m^{-3}), chlorophyll and pheophytin (Chl+Pheo<0.8 mg m^{-3}), and suspended particulate matter (SPM~2 g m^{-3}). Elevated Chl Fl and Chl+Pheo (~2 mg m^{-3}) values measured at mid-depths below the pycnocline defined the subsurface chlorophyll maxima (SCM), which exhibited moderate POC (~10 mmol m^{-3}), c_p (~0.4 m^{-1}) and SPM (~3 g m^{-3}). In contrast, deeper waters below the pycnocline were characterized by low Chl Fl and Chl+Pheo (~0.7 mg m^{-3}), high c_p (>1.5 m^{-1}) and SPM (>8 g m^{-3}) and elevated POC (>10 mmol m^{-3}). POM compositions from surface and SCM regions of the water column were consistent with contributions from active phytoplankton sources whereas samples from bottom waters were characterized by high Pheo/(Chl+Pheo) ratios (>0.4) indicative of altered phytoplankton detritus. Marked contrasts in POM were observed in both surface and mid-depth waters during both cruises. Increases in chlorophyll and POC were measured in mid-depth waters during the September 2016 cruise following a period of downwelling-favorable winds, and in surface waters during the August 2017 cruise following a period of upwelling-favorable winds.

Plain Language Summary

We investigated the distribution and composition of particulate organic matter in waters from the northeast Chukchi Sea during two late summer periods (September 2016 and August 2017). During both cruises we measured a variety of properties (salinity, temperature, density, chlorophyll fluorescence and particle beam attenuation). We also collected individual water samples from specific depths and measured the concentrations of suspended particulate matter, particulate organic carbon and nitrogen, chlorophyll-a and pheophytin (a chlorophyll degradation product). These measurements revealed highly stratified conditions throughout the study area, with surface waters exhibiting relatively low particle and biomass concentrations, mid-depth waters with well-defined subsurface chlorophyll maxima and moderate biomass, and turbid bottom waters with intermediate concentrations of particulate organic carbon and elevated levels of pheophytin. Large contrasts in the composition of particulate materials in both cruises were related to the distribution of different regional water masses. In addition, we observed increases in biogeocemical tracers of phytoplankton production in response to downwelling- and upwelling-favorable wind events. Overall, our work suggests that under the right conditions, phytoplankton production may occur under highly stratified conditions both in surface and sub-surface waters, extending the productive season along Arctic marginal seas.

1 Introduction

Surface warming associated with increased atmospheric CO_2 concentrations is occurring in the Arctic at a pace roughly double the global average (e.g., Allen et al., IPCC 2018), leading to significant decreases in sea ice extent and thickness, and changes in the timing of seasonal melt and re-freeze throughout the Arctic Ocean (e.g., Fetterer et al., 2017; Wood et al., 2015; Stroeve & Notz, 2018). The expansion of the seasonal ice zone and lengthening of the meltwater season have profound implications for the productivity and ecology of the Arctic Ocean (e.g., Grebmeier et al., 2015; Ardyna and Arrigo, 2020; Huntington et al., 2020). Earlier sea ice melt and a longer open-water period can have positive feedbacks on water column conditions that can extend the growing season and result in marked increases in phytoplankton productivity if both nutrients and light are available (e.g., McLaughlin and Carmack, 2010; Zhang et al., 2010; Arrigo et al., 2012; Ardyna et al., 2020).

Remote-sensing based observations indicate increases in the extent and duration of the open water season over the past two decades have contributed to the enhancement in net primary production along Arctic marginal seas over this period (Lewis et al., 2020; Arrigo and van Dijken, 2015). Analyses by these authors suggest that the observed increases in net primary production over the past ten years are driven by enhanced phytoplankton biomass, indicating that increases in nutrient supply are required to support the observed productivity increases. In inflow shelves, such as the Chukchi Shelf, advection of nutrients from the Pacific may contribute to these trends. Work by Woodgate (2018) based on mooring data from the Bering Strait indicated an increase in the

Pacific inflow to the Arctic Ocean, which could represent a source for enhanced nutrient input. However, more recent studies suggest there is significant interannual variability in the northward transport across Bering Strait (e.g., Nguyen et al., 2020) and no clear long-term trends in the supply of nutrients from the Pacific (e.g., Danielson et al., 2021).

Enhancement in the vertical mixing of nutrients into the euphotic zone is another mechanism that can explain increases in net primary productivity, especially in the shallow Arctic shelves and marginal seas (see review by Ardyna and Arrigo, 2020). In terms of predicting the effects of climate change on Arctic Ocean ecosystems, it important to understand how physical drivers (e.g., stratification and mixing) control key biogeochemical processes (e.g., dissolved nutrient supply) that impact primary productivity (e.g., Slagstad et al., 2015). For example, at an Arctic-wide scale, increased warming and greater inputs of melt water and river runoff are likely to enhance stratification in the euphotic zone, which can result in nutrient depletion in the late season and potentially decreased overall productivity despite increases in light availability (e.g., Yamamoto–Kawai et al., 2009; Jackson et al., 2011). On the other hand, longer periods of open water over of Arctic marginal seas may enhance current- and wind-driven mixing (e.g., Pickart et al., 2013; 2019; Danielson et al., 2014; 2017; Lin et al., 2019; Foukal et al., 2019) that can inject nutrients into the euphotic zone. Recent studies indicate that episodic mixing and inputs of nutrients along geographic and bathymetric features such as capes, canyons and shelf margins can drive phytoplankton productivity and increases in biomass within surface waters during the open water season (e.g., Juranek et al., 2019; Goñi et al., 2019). Additionally, the prolonged ice-free conditions in late summer and fall can lead to enhanced wave resuspension and coastal erosion, which mobilize reactive materials from the nearshore that can fuel secondary production and nutrient cycling (e.g., Bröder et al., 2019; Vonk et al., 2015).

In this study, we present hydrographic properties and particulate organic matter (POM) distributions in waters along the northeast region of the Chukchi Sea shelf during two late summer-early fall cruises in 2016 and 2017. We investigate the role that stratification and bathymetric features have on influencing POM concentrations and compositions, and examine the impacts of both downwelling- and upwelling-favorable wind events along different regions of the Chukchi Shelf, including areas around Hannah Shoal and Barrow Canyon. We focus specifically on sub-surface distributions that were not evident from our previous studies of surface trends (e.g., Juranek et al., 2019; Goñi et al., 2019). Our efforts contribute to an increased understanding of mechanisms of enhanced productivity during the open-water season and provide additional insights into potential biogeochemical impacts of increased and prolonged sea ice loss in marginal Arctic seas.

2 Background and Methods

2.1 Study area

The Chukchi Sea is located directly north of the Bering Sea and constitutes the gateway between the Pacific and Arctic Oceans (Figure 1a). Several regional water masses, including Anadyr Water, Bering Shelf Water and Alaska Coastal Water, enter the Chukchi Shelf through Bering Strait, with their inflow being regulated by sea level differences between the Pacific and Arctic and regional wind forcings (e.g., Coachman et al., 1975; Weingartner et al., 2005; Woodgate et al., 2015; Danielson et al., 2014; 2017 and references therein). While the mean flow is from the Pacific to the Arctic, once inside the Chukchi Sea circulation is largely topographically-steered along three primary pathways: a western branch through Herald Canyon; a Central Channel pathway between Herald and Hannah Shoals; and an eastern branch along the Alaskan coast (e.g., Danielson et al., 2017). This latter coastal pathway is typically the fastest to transport materials to the Beaufort Sea, whereas the other two pathways are significantly slower and can take several months to traverse the Chukchi Shelf (e.g., Shroyer and Pickart, 2019). Significant physical and biogeochemical modifications of these inflow waters occur during their transit to the Beaufort Sea, fundamentally impacting the biogeochemistry and ecology of this inflow shelf (e.g., Arrigo et al, 2014; Grebmeier et al., 2015).

The major water masses entering the Chukchi Sea have distinct characteristics, with Anadyr Water having significantly higher dissolved nutrients than Bering Shelf Water and Alaska Coastal Water (ACW), the latter of which also tends to be fresher (e.g., Coachman et al., 1975; Arrigo et al., 2014). During winter, waters in the northern Bering and Chukchi Sea can undergo complete mixing due to sea ice formation and brine rejection, resulting in cold ($T < 0$ C), salty ($S >$ 30 to 33.5), dense and nutrient-rich waters that are identified as Bering-Chukchi Winter Water (BCWW; Danielson et al., 2017). These winter waters can be further differentiated based on temperature (e.g., Pacini et al., 2019) into colder, newly ventilated winter water ($<$ -1.6 C) and warmer ($>$ -1.6 C) remnant winter water. In the spring and early summer, water column stratification due to warming, sea ice melt and river discharge (e.g., Weingartner et al., 2017), facilitates phytoplankton growth and drawdown of dissolved nutrients within the euphotic zone (e.g., Arrigo et al., 2014; Brown et al., 2015). The warming throughout the summer season over the Pacific Arctic region results in relatively warm ($T > 0$ C) waters that can be classified as Bering-Chukchi Summer Water (BCSW; Danielson et al., 2017). Other water masses observed along the Chukchi Sea during the spring and summer seasons include Melt Water (MW), which describes lower salinity ($S < 30$), high-buoyancy waters directly influenced by seasonal sea ice melt; as well as the warmer ($T > 7$ C) ACW, which because of its circulation path can remain as a discernible water mass along the Alaskan coastline (e.g., Danielson et al., 2017).

The strongly advective regime that characterizes the Chukchi Shelf is influenced by seasonal processes that affect light and nutrient availability and impact overall productivity (e.g., see review by Ardyna and Arrigo, 2020 and references therein). Thus, the Chukchi Sea exhibits a strong seasonal cycle of productivity that starts in the spring (May and June) with ice-algae and under-ice plankton blooms and develops into a two-layer open water system with strong nutrient-depletion that limits surface productivity later in the summer (July to September). Our study is designed to investigate the distribution of POM in the northeastern Chukchi shelf during this latter period and evaluate the role of physical forcings in its production and fate.

a)

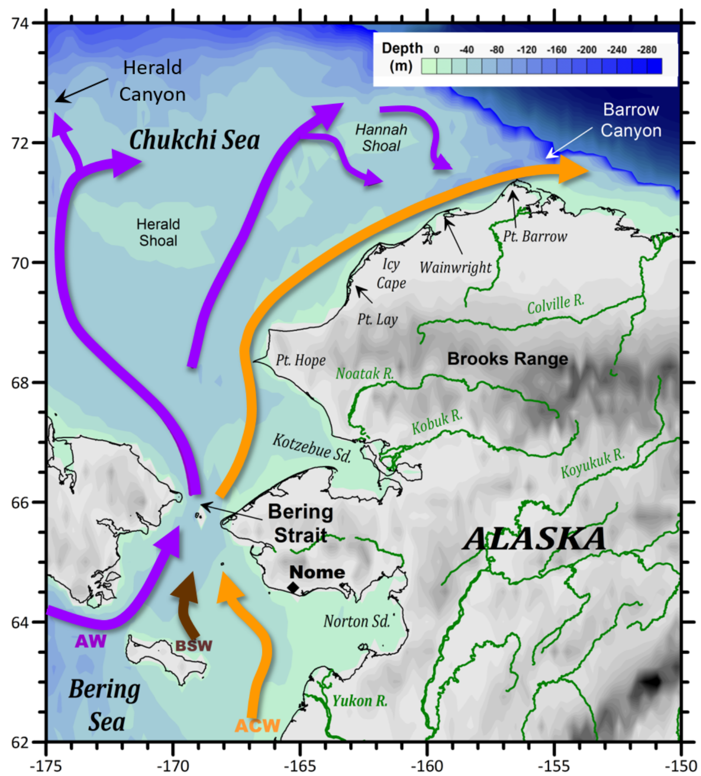

b) **c)**

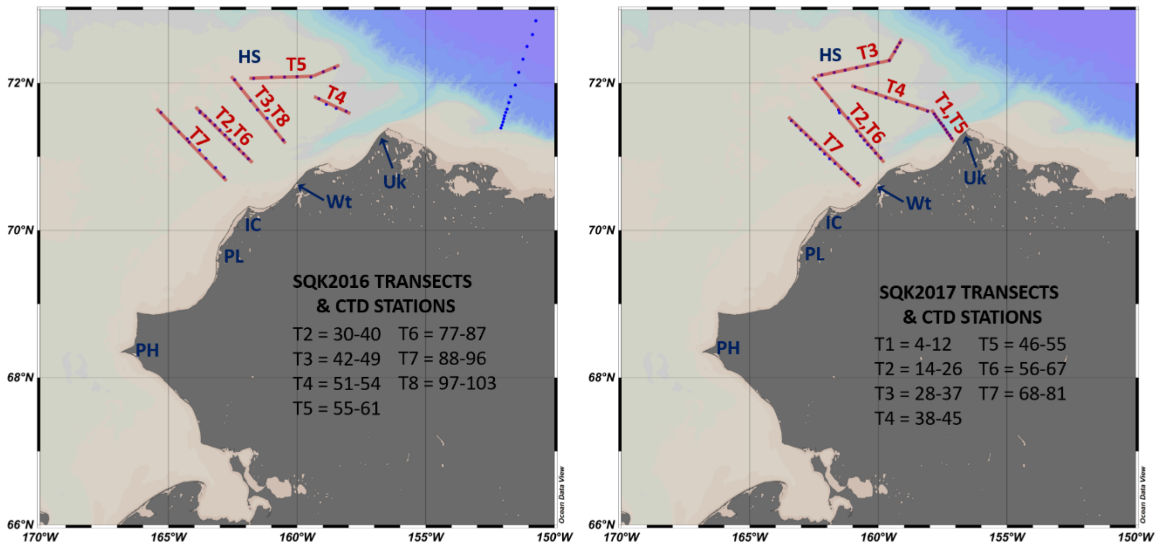

Figure 1. Maps of the study area highlighting a) regional circulation and bathymetry; b) CTD stations and transects occupied SKQ201612S and c) CTD stations occupied during SKQ201712S. Transect and station numbers for both cruises are listed. Note that based on the location of the Distributed Biological Observatory array (e.g., Grebmeier et al., 2019), transects 2 and 6 in SKQ201612S coincided with the DBO4 line, whereas in SKQ201712S, transects 1 and 5 coincided with the DBO5 line and transect 7 coincided the DBO4 line.

2.2 Oceanographic cruises

In September of 2016, we sailed aboard the R/V Sikuliaq from Nome, AK, to the northeast Chukchi Sea and carried out oceanographic measurements and sampling along several cross-shelf transects (Figure 1b). During this period (Sep 3-25, 2016) we were able to occupy repeated transects along the established (e.g., Grebmeier et al., 2019) DBO4 line (transects 2 and 6) and off Wainwright (transects 3 and 8). This cruise (SKQ201612S) took place during a period of critical subsistence hunting of marine mammals by several coastal communities along Alaska's North Slope. To avoid interference with these activities and following best practice guidelines (e.g., Konar et al., 2017), the ship was kept $>$ 30 nautical miles offshore from established whaling grounds. In 2017, we conducted a second cruise (SKQ201712S) aboard the R/V Sikuliaq and occupied several transects along our study area from August 7-21, 2017 (Figure 1c). During this campaign, we were able to carry out repeated occupations along two transects, one offshore from Pt. Barrow (Transects 1 and 5), which coincided with the location of the DBO5 line, and one offshore from Wainwright (Transects 2 and 6). Because this cruise did not interfere with subsistence hunting efforts, we were able to extend the 2017 transects much closer to shore, including transect 7 that coincided with the location of the DBO4 line. During both cruises, spaced hydrographic stations were occupied along each transect. At each station, the ship's CTD-rosette system was deployed to conduct a variety of sensor-based measurements during the down cast and to collect water samples at selected depths during the up cast.

2.3 Ancillary data

Wind and atmospheric pressure data were downloaded from NOAA's Barrow Meteorological station (https://www.esrl.noaa.gov/gmd/obop/brw/) for the periods around each cruise. We used wind magnitude and direction to calculate the east-west (Uwind) component of the wind speed, which reflects upwelling-favorable (easterly winds) and downwelling-favorable (westerly winds) conditions along Alaska's north slope margin (e.g., Pisareva et al., 2019; Pickart et al., 2019; Foukal et al., 2019).

2.4 Methods

2.4.1 CTD and optical sensor data

Temperature (C) and conductivity measurements were collected using a Sea-Bird 911 CTD instrument package and used to calculate salinity and density ($_t$, kg m^{-3}). Measurements of photosynthetically active radiation (PAR; Ein cm^{-2} s^{-1}), chlorophyll fluorescence (Chl Fl; mg m^{-3}) and particle beam attenuation (c_p; m^{-1}) were obtained using sensors mounted on the CTD rosette (Biospherical QSP-240, Wet Labs ECO FL Fluorometer, and Wet Labs C-Star 25-cm transmissometer, respectively). All sensors were calibrated prior to each cruise, and cleaned and rinsed with distilled water after each cast. All sensor-based measurements were conducted during both the down- and up-cast at each station. Down-cast data were binned at 1 meter intervals to produce water column profiles at each station, which were then gridded and interpolated by kriging techniques using the software package Surfer (Golden Software). To account for the spatial scale differences of the data sets (i.e., depth in meters vs. distance along transect in kilometers), the gridding was conducted using a 3:1 anisotropy ratio to construct the contoured transects presented below. Up-cast data were averaged for each Niskin bottle deployment and used to calculate temperature, salinity, $_t$, PAR, Chl Fl and c_p values for each of the water samples that were collected using the CTD rosette.

2.4.2 Collection and analyses of individual water samples

Water samples were collected from specific depths using Niskin bottles mounted on the CTD rosette. For the most part we collected samples from the surface, mid- and bottom sections of the water column, often targeting features in Chl Fl and c_p to capture particle variability throughout the water column. Niskin bottles were sampled immediately after the CTD package was brought up on deck and variable volumes of water vacuum were filtered onto different-diameter glass fiber GF/F filters (nominal pore size of 0.7 m) to isolate suspended particles using established procedures (e.g., Chaves et al., 2021). In order to collect large amounts of particles, we filtered between 2 to 4 liters of individual water samples through pre-combusted, pre-weighed 47-mm diameter GF/F filters.

For particulate organic carbon and nitrogen analyses, 200 to 500 ml of water were filtered through pre-combusted 13-mm diameter GF/F filters, whereas for pigment analyses we used pre-combusted 25-mm diameter GF/F filters. Water samples that had undergone filtration through GF/F filters were filtered again on a periodic basis and these samples used to estimate the mass of salt in the filter as well as carbon and nitrogen blanks associated with sorption of dissolved organic matter (e.g., Goñi et al., 2019; Chaves et al., 2021). All filter samples were kept frozen (-80 C) until analyses.

The dry mass concentration of suspended particulate matter (SPM; g m^{-3}) in each 47-mm filter sample was determined by weighing the dry filter, subtracting the original mass of the filter, applying a mass correction, and dividing by the volume filtered. We note that because of concerns associated with rupturing cell membranes and potentially losing materials from the filters, we did not include a deionized water rinse step to remove salt (e.g., Stramski et al., 2007). Instead we used the SPM-particle beam attenuation relationships observed (Figure S1) to determine background mass gain following filtration, which is primarily due to the presence of residual salt (e.g., Stavn et al., 2009). The magnitude of the c_p-based correction was comparable to SPM determinations from the filtration of selected pre-filtered samples. While we recognize the challenges of determining the mass of total suspended solids in salt water samples (e.g., Stavn et al., 2009), the SPM data presented here provide insight into the distribution of suspended particulate materials in the study area.

Particulate organic carbon (POC) and particulate nitrogen (PN) concentrations (mmol m^{-3}) in water samples were measured by analyzing 13-mm GF/F filter samples according to established techniques (see Goñi et al., 2019; Chaves et al., 2021). Briefly, the procedure involves exposing filter samples placed in silver boats to hydrochloric acid fumes over 24 hours to remove inorganic carbon, drying the samples for another 24-hour period and then wrapping the silver boats into tin boats for CN analyses by high temperature combustion. Samples and blanks associated with dissolved organic matter (DOM) sorption were analyzed in the same manner and the average carbon and nitrogen contents of the DOM blanks used to correct the measured values for POM samples. During each cruise, DOM-associated blanks were collected at surface, mid- and near-bottom depths of the water column and the averages applied to correct samples from each respective depth. POC and PN concentrations were calculated by dividing the blank-corrected carbon and nitrogen contents of each filter by the total volume of water filtered.

Chlorophyll (Chl) and pheophytin (Pheo) concentrations (mg m^{-3}) were analyzed by extracting the filters in 8 mL of a 90% acetone solution at 4 °C overnight. The samples were then measured using a Turner Design Model 10-AU fluorometer according to the acid addition method (Parsons et al.1984; Arar and Collins 1997) with a detection limit of 0.025 mg m^{-3}.

3 Data availability

All the data, including CTD profiles and individual sample compositions from Niskin bottles are archived in the Arctic Data Center (pending doi's; in the meantime, see supplement Tables S1 and S2). All the CTD profile data are available at the Rolling Deck to Repository (R2R) data repository for R/V Sikuliaq's cruises SKQ201612S and SKQ210712S (https://www.rvdata.us/search/cruise/SKQ201612S12S and https://www.rvdata.us/search/cruise/SKQ201712S12S, respectively.

4 Results

4.1 Sea ice and atmospheric conditions

During SKQ201612S, we encountered significant amounts of sea ice above latitudes of 72 degrees north, which limited our operations in the area north and east of Hannah Shoal. In contrast, during SKQ201712S, the sea ice edge was well to the east and north of our study area and thus we had no limitations in operations.

Measurements from the meteorological station at Pt. Barrow provide a regional context to the atmospheric conditions during each cruise (Figure 2). For example, SKQ201612S took place during a period in September characterized by highly variable, moderate winds (5 to 20 knots) that included short periods of easterlies (upwelling-favorable) and westerlies (downwelling-favorable) (Fig. 2a). A period of high (peak winds > 20 knots) downwelling-favorable winds occurred between September 17-20, which provided a chance to compare conditions before and after the wind event by re-occupying transects along the DBO4 line and off Wainwright (Transects 2 and 6 and Transects 3 and 8, respectively; Fig. 1b). Conditions during SKQ201712S were characterized by markedly lower wind speeds, which rarely exceeded 15 knots (Fig. 2b). A switch from downwelling-favorable winds (positive U_{wind} speeds) to upwelling favorable winds (negative U_{wind} speeds) occurred around August 12 and lasted several days, which allowed us to compare conditions under contrasting wind forcings by evaluating distributions across Barrow Canyon (DBO5 line) and off Wainwright (Transects 1 vs. 5 and Transects 2 vs. 6, respectively; Fig. 1c).

4.2 Hydrographic properties and particle distributions

The hydrographic CTD surveys during the two cruises focused on the eastern Chukchi Shelf. Chlorophyll fluorescence (Chl Fl) and particle beam attenuation (c_p) measurements from sensors mounted on the CTD package, combined with measured concentrations of particulate organic carbon (POC) and the photosynthetic pigments chlorophyll and pheophytin (Chl and Pheo, respectively), allowed us to explore particulate material distributions throughout the water column under different conditions. Here, we present contoured hydrographic (temperature, salinity and density) and Chl Fl and c_p sensor data along with superimposed POC, Chl+Pheo, and SPM concentrations from individual bottle samples to illustrate trends in POM distributions during both late-season cruises. Table 1 provides a summary of the bottle data from both SKQ201612S and SKQ201712S individual water samples from the three depth intervals routinely sampled. Distributions of PN concentrations showed similar trends to those of POC and are presented in the supplementary information (Tables S1 and S2). PAR profiles are shown for selected CTD stations occupied during daylight hours to document light availability throughout the water column during both cruises.

a)

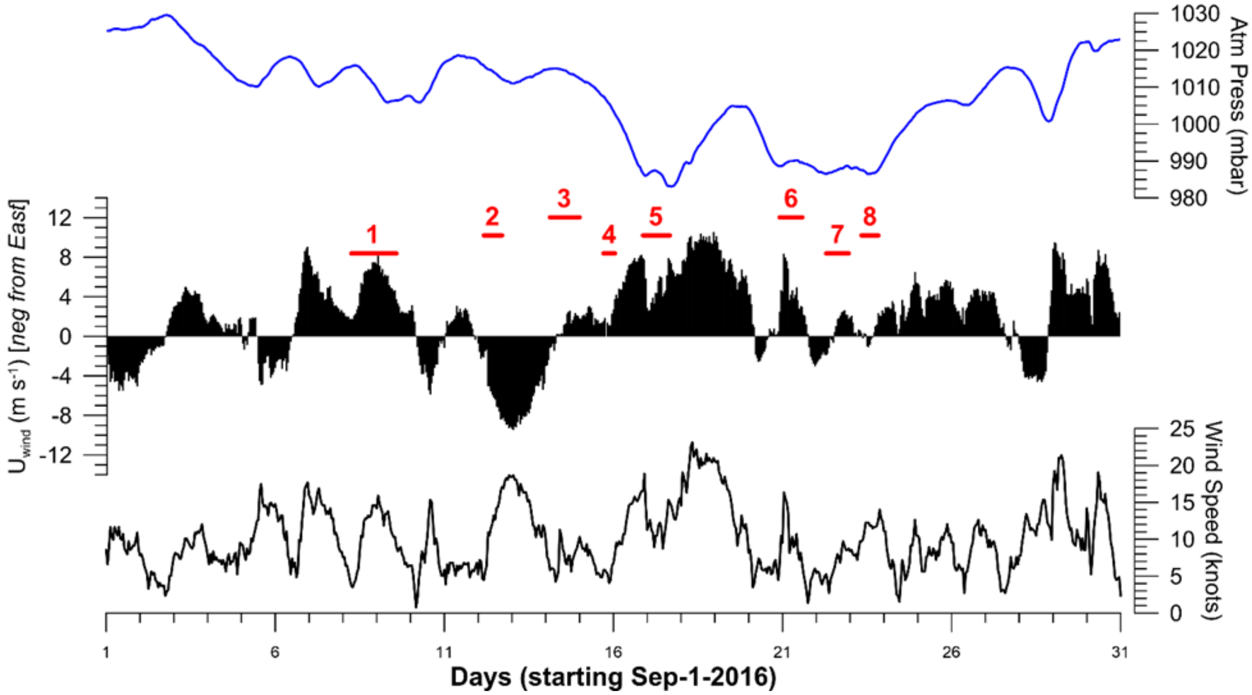

b)

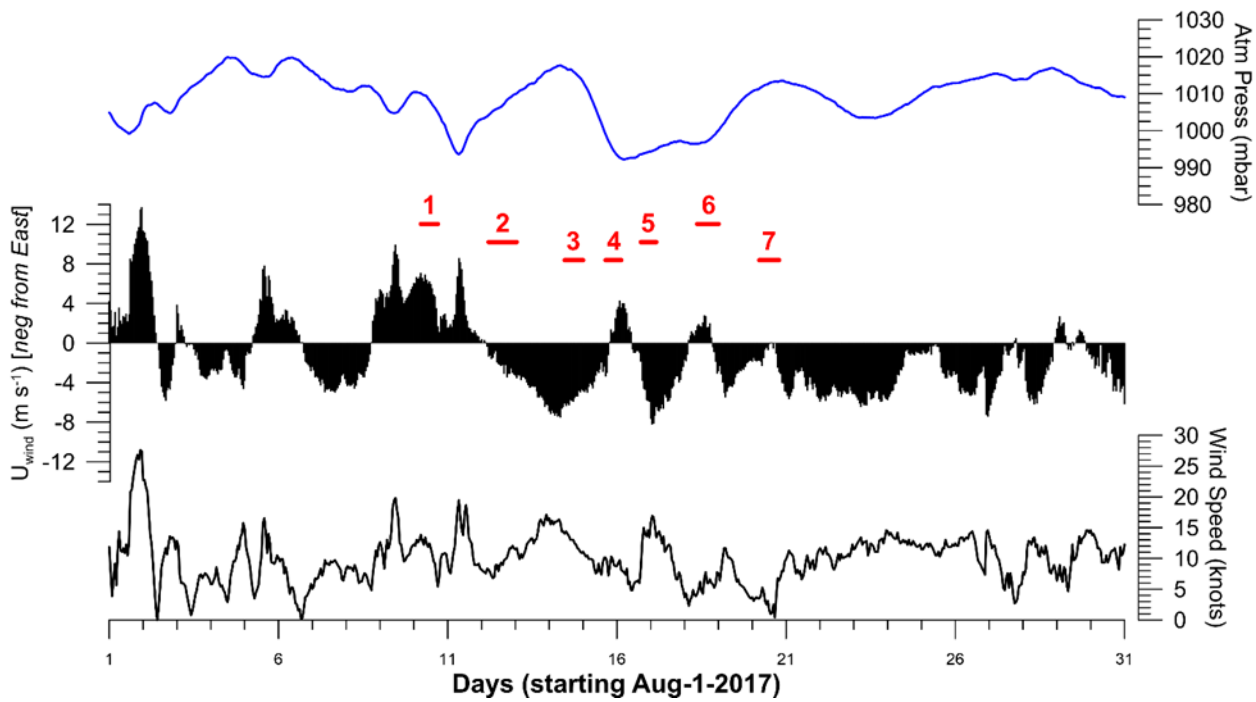

Figure 2. Atmospheric measurements from Pt. Barrow Meteorological station during a) SKQ201612S and b) SKQ201712S cruise periods. The data plotted include overall wind speed (knot), east-west wind speed (m s^{-1}), and atmospheric pressure (mbar). The timing and duration of CTD transects (see Figure 1 b, c) are shown to provide context to oceanographic observations. All NOAA met data are available at https://www.esrl.noaa.gov/gmd/obop/brw/.

4.2.1 SKQ201612S (Sep 12-23, 2016) Transects

The salinity and temperature distributions along the seven transects completed during the 2016 cruise are presented in Figure 3. As it is evident from these plots, the water column in the study area was highly stratified, primarily due to the large contrasts in salinity, with the top 10 to 20 m of the water column displaying low to intermediate salinities of (26 to 28), whereas the deeper sections were characterized by higher values (28-30). The temperature signatures displayed much less vertical variability with surface waters (0-20 m) exhibiting temperature ranges (-1 to 2 C) that were comparable to those in deeper waters (Fig. 3). There were several noticeable spatial and temporal trends. For example, cold, fresher surface waters were most predominant in the transects from the northeast region of the study area (e.g., transects 4 and 5) whereas the inshore sections of transects in the southwestern section were characterized by higher salinities (~29) and temperatures (3 to 4 C).

There was some variability in hydrographic distributions between transects occupied prior and following the downwelling-favorable wind event (Sep 17-20, 2016). For example, minimal changes in temperature and salinity were detected along transects 3 and 8, which were located within the central part of the study area. However, we measured slight increases in both variables over the top 20 m of water column at the 50 km CTD station along transect 8 (Fig. 3). Further to the west, transect 6 showed markedly elevated temperatures and salinities in surface waters following the wind event relative to values measured along transect 2 that covered the same geographical locations prior to the wind event. Transect 7, which was located in the western-most section of the study area and was occupied following the downwelling-favorable wind event, displayed markedly higher salinities and temperatures in surface waters throughout the transect. Overall, while these contrasts reflect spatial variability in surface water masses along this highly advective region of the Pacific Arctic, it is likely the wind event of September 17-20, 2016 led to lateral and vertical mixing of water masses that contributed to the trends observed.

The density distributions plotted in Figure 4 confirm the highly stratified conditions during SKQ201612S, especially along the northeast region of the study area (transects 4 and 5), where a very steep pycnocline was evident between 15 to 20 m water depth. Also evident in these plots were the contrasts in surface densities along transects occupied prior and following the wind event (e.g., transect 2 vs. 6, respectively) and the lack of major changes in density in the deeper regions of the water column below ~ 20 m. Data from individual water samples plotted in Figure 4 show POC concentrations ranged from 2 to 20 mmol m^{-3} throughout the water column of the seven transects occupied, with a high degree of variability in samples collected from surface and pycnocline depths. POC concentrations were quite low (< 5 mmol m^{-3}) in many of the surface samples, with higher (10 to 20 mmol m^{-3}) values measured at locations that exhibited fronts associated with lateral density contrasts. Samples collected at depths near the pycnocline (24 < $_t$ < 25.5 kg m^{-3}) also displayed significant variability, with most transects displaying intermediate POC values (5 to 10 mmol m^{-3}). The DBO4 transects west of Wainwright (transects 2 and 6) included several samples displaying markedly higher POC concentrations (10 to >30 mmol m^{-3}). In contrast, samples from the pycnocline along transects directly off Wainwright (transects 3, 8) were characterized by low POC values (< 5 mmol m^{-3}). The majority of samples collected from the higher-density waters ($_t$ > 25.5 kg m^{-3}) that occupied the deeper regions of the water column along all seven transects displayed moderately elevated POC concentrations (10 to 15 mmol m^{-3}), with the major exception being the samples from the shallower sections around Hannah Shoal, which displayed markedly lower (> 5 mmol m^{-3}) POC concentrations (Fig. 4).

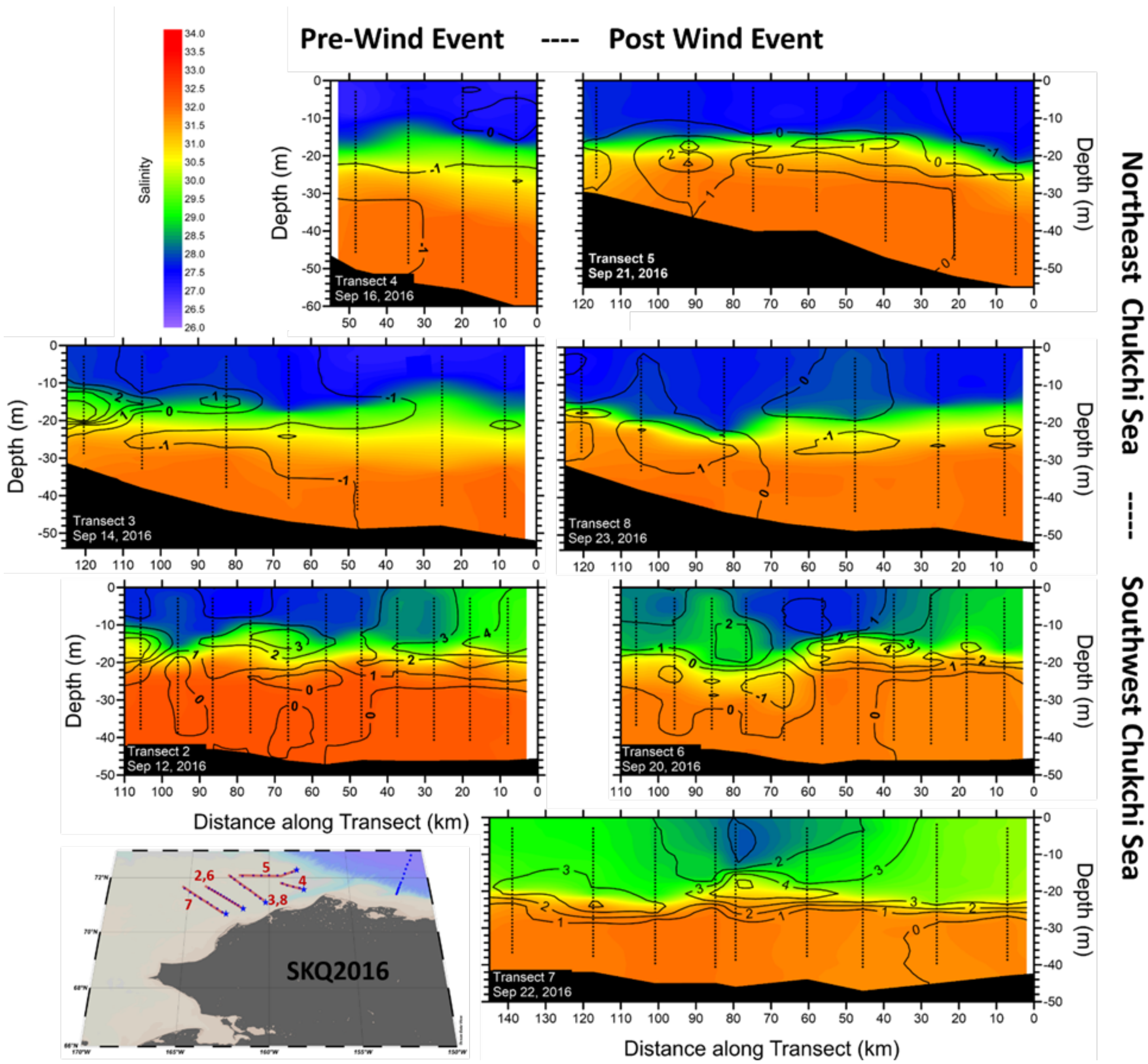

Figure 3. Distributions of salinity and temperature (°C) throughout the water column across the seven hydrographic transects completed during SKQ201612S. Note that the start of each transect is identified by a blue star in the map insert. The cross-section contour plots are based on binned downcast data collected at each CTD station indicated by dotted lines in each transect.

Contour plots of Chl Fl along all seven transects are shown with the combined pigment (Chl+Pheo) concentrations measured in individual water samples superimposed in each panel (Figure 5). As can be seen from these plots, all transects displayed relatively low Chl Fl signals (< 1.0 mg m^{-3}) throughout most of the water column except for the sub-surface chlorophyll maxima (SCM) located between 20 to 30 meters of water depth. The DBO4 transects west of Wainwright (transects 2 and 6) were characterized by the most intense SCM, with peak fluorescence signals consistent with Chl concentrations > 3 mg m^{-3}. In contrast, other transects, such as transects 4 and 7, were characterized by more muted SCM that did not extend along the whole transect distance. In all cases, SCM were located at depths directly below the pycnocline, typically within $_t$ ranges between 24.5 and 25.5 kg m^{-3}. The Chl Fl signals in both surface and deep waters ranged from < 0.4 to moderate values around 1.5 mg m^{-3} and varied within and among transects. Combined pigment (Chl+Pheo) concentrations from individual water samples were conducted in selected transects (transects 2, 3, 4, and 5) and for the most part agreed well with the Chl Fl patterns, including the high values (> 2 mg m^{-3}) measured along specific locations of the SCM in transects 2 and 3.

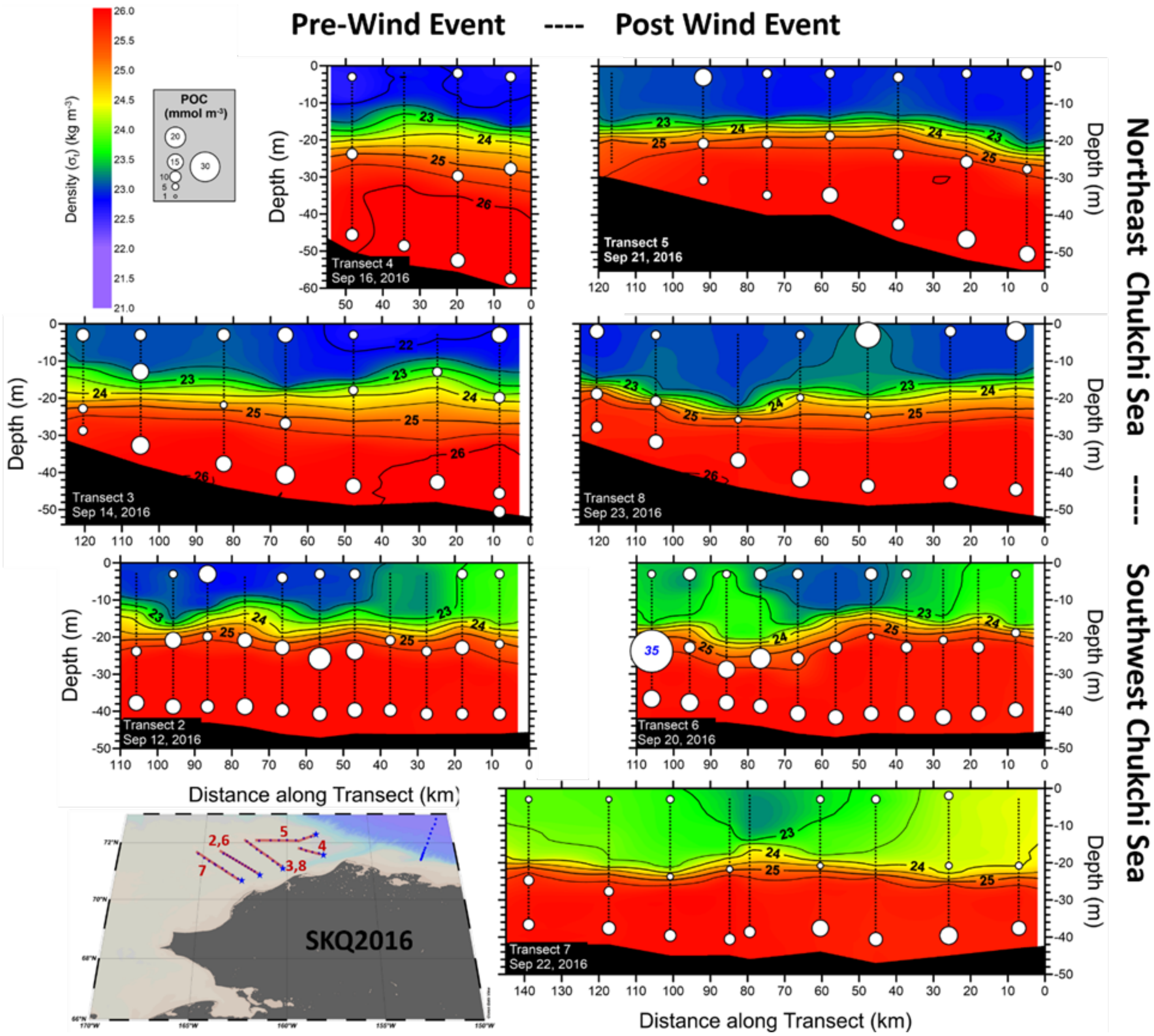

Figure 4. Distributions of density ($_t$; kg m^{-3}) throughout the water column and particulate organic matter concentrations (POC; M) from individual samples collected across the seven hydrographic transects completed during SKQ201612S. Note that the start of each transect is identified by a blue star in the map insert. The cross-section contour plots are based on binned downcast data collected at each CTD station indicated by dotted lines in each transect. The bubble plots showing POC concentrations are superimposed on the contour maps to identify the location of each individual sample.

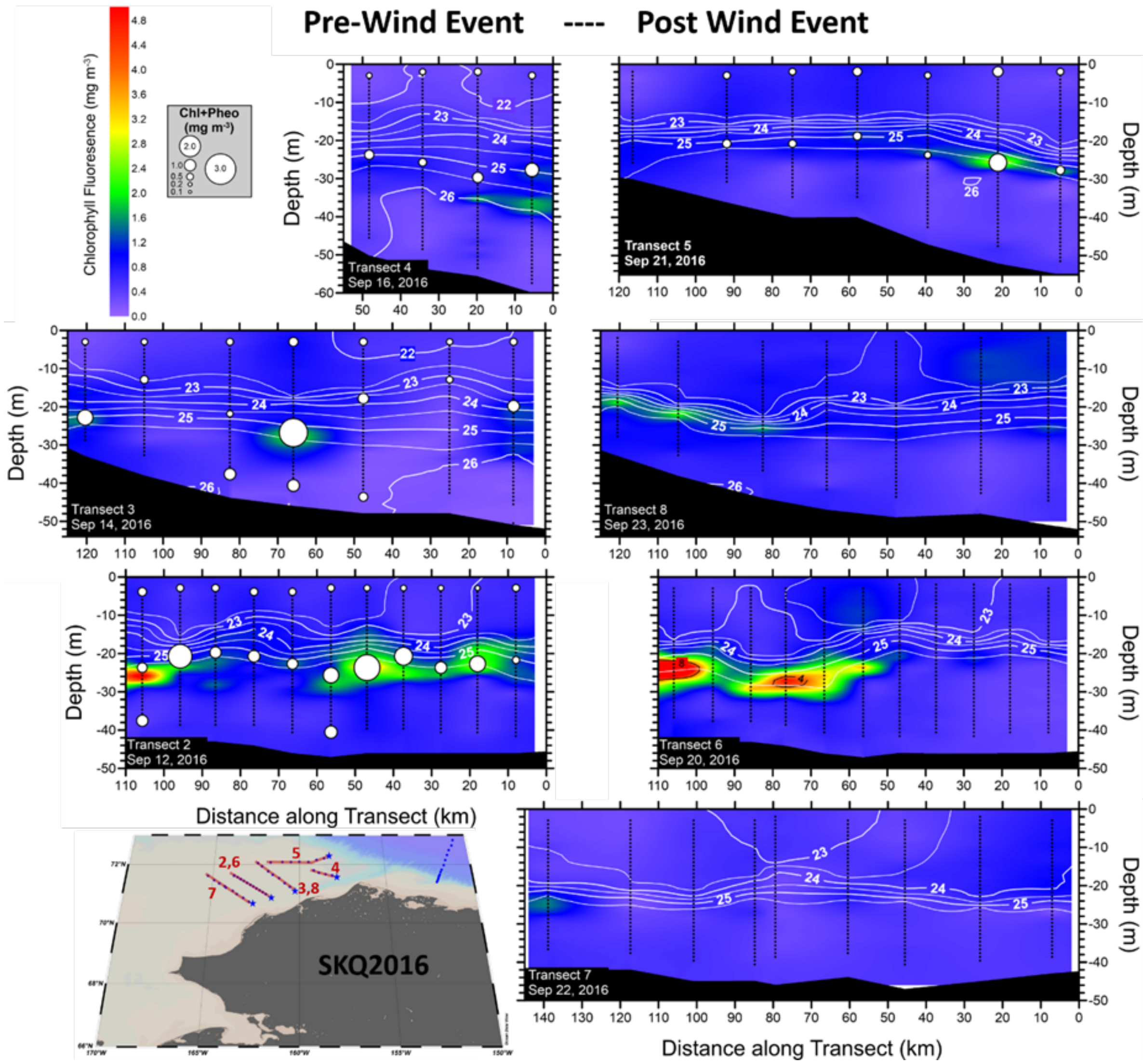

Figure 5. Distributions of chlorophyll fluorescence sensor measurements (Chl Fl; mg m^{-3}) throughout the water column and combined photosynthetic pigment concentrations – chlorophyll and pheophytin (Chl+Pheo; mg m^{-3}) – from individual samples collected across the seven hydrographic transects completed during SKQ201612S. Note that the start of each transect is identified by a blue star in the map insert. The cross-section contour plots are based on binned downcast data collected at each CTD station indicated by dotted lines in each transect. The bubble plots showing Chl+Pheo concentrations are superimposed on the contour maps to identify the location of each individual sample.

Further insights into the distribution of suspended particles along the water column of the northeast Chukchi Shelf can be obtained from the contoured distributions of c_p signals along all seven transects (Figure 6). In this figure we also superimposed the SPM concentrations obtained from individual water samples collected using the CTD-rosette system. As is evident from these plots, the water column in this region of the Chukchi Sea during the cruise period exhibited marked contrasts in particle distributions and overall turbidity, with all surface waters at and above the pycnocline displaying c_p values of < 0.4 m^{-1}, whereas bottom waters below the pycnocline were characterized by markedly elevated c_p values of 1 to over 2.5 m^{-1}. The stark contrasts in c_p were corroborated by the distributions of SPM concentrations from different depths, which showed low concentrations (SPM < 3 g m^{-3}) in surface waters at and above the pycnocline and elevated concentrations ($5 >$ SPM > 15 g m^{-3}) in bottom waters below the pycnocline. Based on c_p and SPM distributions before and after the period of downwelling-favorable winds (e.g., transects 2 vs. 6 and 3 vs. 8, respectively) there were changes in the overall turbidity of the water column that may have been related to this wind forcing. For example, there were increases in both c_p values and SPM concentrations in the regions of the water column below the pycnocline along transects 6 and 8 compared to transects 2 and 3, which were consistent with elevated particle concentrations following the September 17-20 wind event.

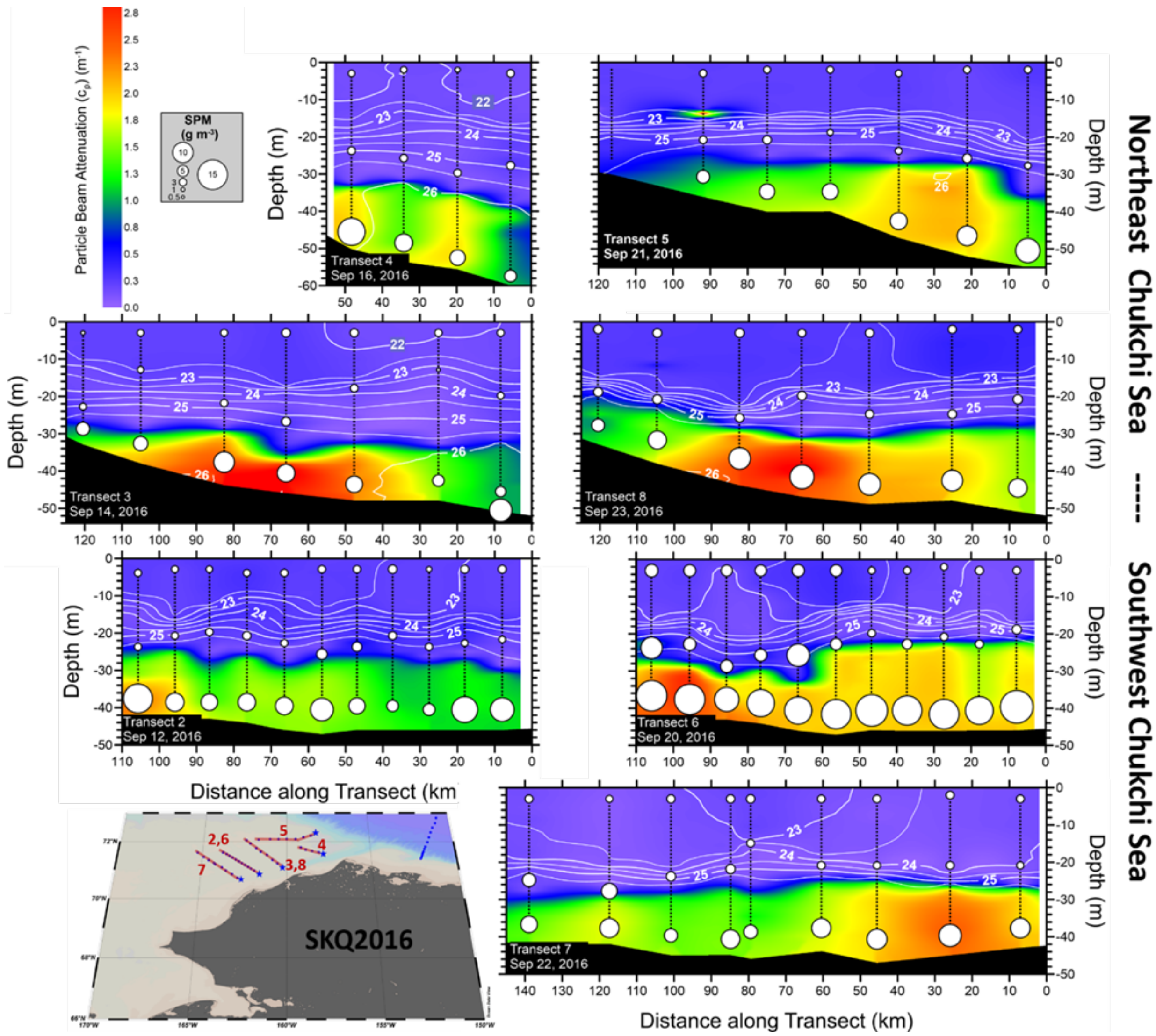

Figure 6. Distributions of particle beam attenuations sensor measurements (c_p; m^{-1}) throughout the water column and combined suspended particulate matter concentrations (SPM; g m^{-3}) from individual samples collected across the seven hydrographic transects completed during SKQ201612S. Note that the start of each transect is identified by a blue star in the map insert. The cross-section contour plots are based on binned downcast data collected at each CTD station indicated by dotted lines in each transect. The bubble plots showing SPM concentrations are superimposed on the contour maps to identify the location of each individual sample.

To illustrate the light conditions throughout the water column during the cruise,

Figure 7 shows the profiles of PAR relative to surface values for three stations that were occupied around noon local time, when surface PAR was 550-570 Einsteins cm^{-2} s^{-1}. Steep light attenuation characterized the water column along the Chukchi Shelf, with less than 10% of surface PAR reaching below 15 m of water depth. However, it is clear that at the height of daylight, more than 1% of surface PAR (often used to define the euphotic zone; e.g., Ardyna et al., 2013) penetrated below the pycnocline. Many of the CTD stations were occupied during nighttime operations, so we were not able to conduct a comprehensive survey of daily PAR profiles that would have allowed a full characterization of the light regime during the cruise.

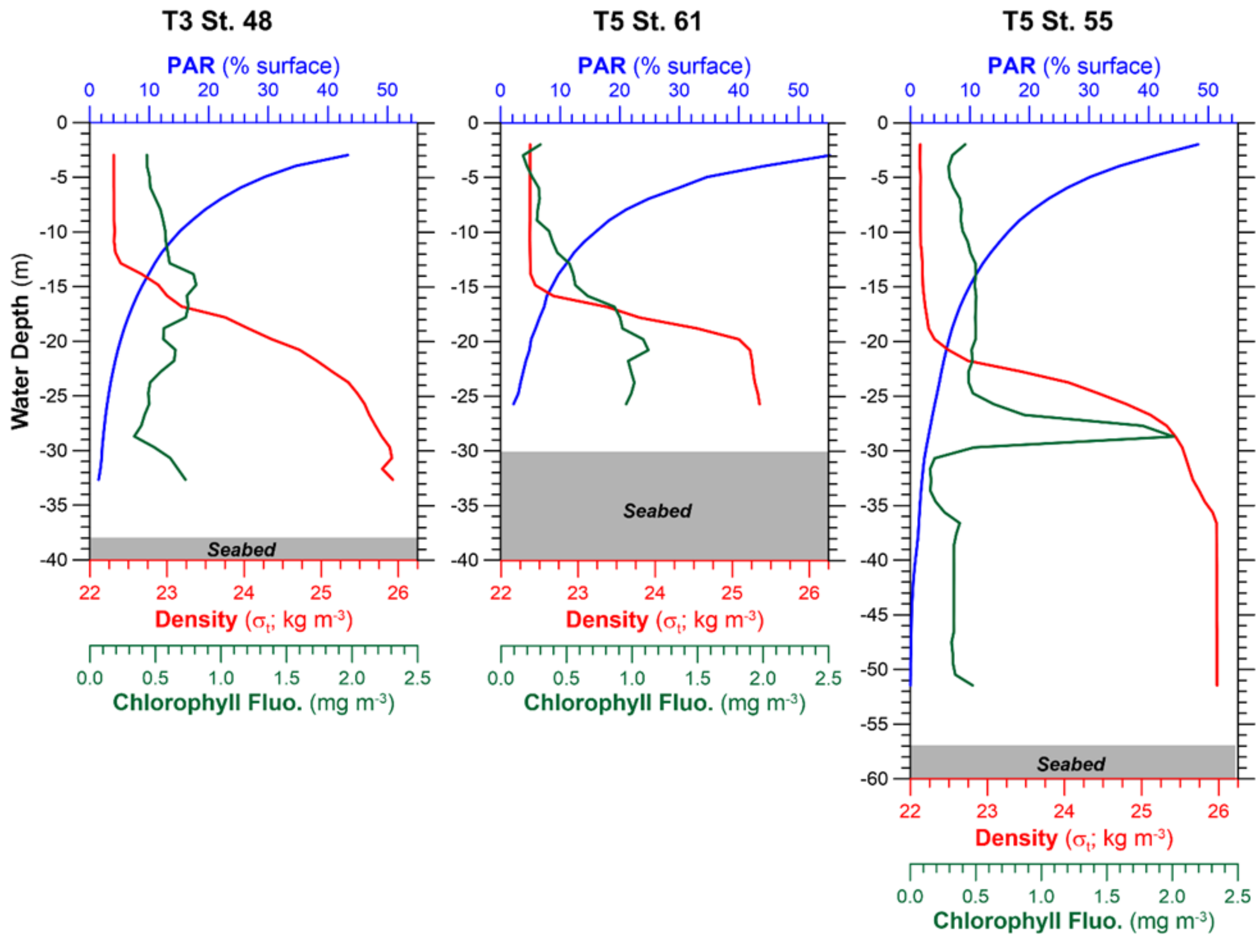

Figure 7. Profiles from selected hydrographic stations identified by transect (T#) and CTD station (St.#) numbers (see Figure 1) occupied near local midday during SKQ201612S. Local date/time occupation of these hydrographic stations is as follows: T3 St.48, September 14, 2016 at 12:30; T5 St.55, September 16, 2016 at 12:54; T5 St.61, September 17, 2016 at 12:21. The figures show

depth profiles of density ($_t$; kg m^{-3}), chlorophyll fluorescence (mg m^{-3}) and photosynthetically active radiation (PAR; Ein cm^{-2} s^{-1}) measurements calculated as a percent of surface PAR

4.2.2 SKQ201712S (Aug 10-20, 2017) Transects

The 2017 Sikuliaq cruise occupied similar locations to the 2016 cruise but, because it did not conflict with the subsistence harvest season, we were able to extend the transects closer to shore (Fig. 1c). As was the case for the SKQ201612S, we illustrate water column distributions during SKQ201712S by showing contour plots for the different transects organized to show both spatial and temporal variability, the latter highlighting contrasts before and after the upwelling-favorable wind event during August 12-17, 2017 (Fig. 2b).

Hydrographic data from all seven transects occupied during SKQ201712S (Figure 8) show that, in contrast to SKQ201612S, the water column of the northeast Chukchi Shelf in August of 2017 was characterized by relative uniform salinities and a larger range of temperatures. For example, SKQ201712S salinities varied between 29 and 34, with only surface waters from the most offshore station in transect 1 displaying salinities lower than 29.

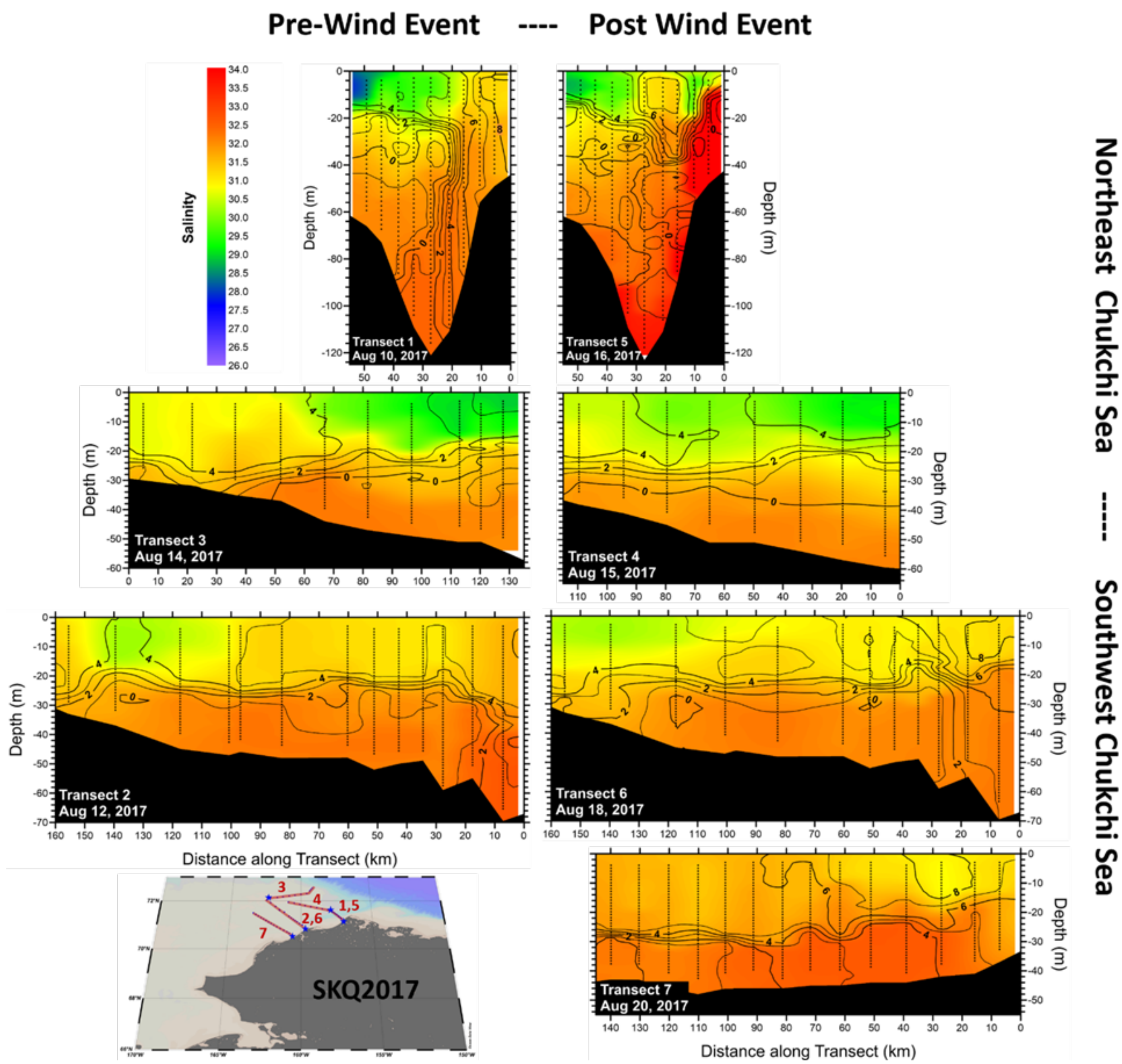

Figure 8. Distributions of salinity and temperature (°C) throughout the water column across the seven hydrographic transects completed during SKQ201712S. Note that the start of each transect is identified by a blue star in the map insert. The cross-section contour plots are based on binned downcast data collected at each CTD station indicated by dotted lines in each transect

Temperature conditions through the water column of all seven transects showed a broad range in values from -1 to 8 C. Surface waters were characterized by significantly warmer temperatures than deeper waters resulting in stratified conditions that, in contrast to SKQ201612S cruise, were much more temperature-controlled as opposed to salinity-controlled. As can be seen in Table 1, the stark contrasts in salinity and temperature distributions between the two cruises was primarily caused by the diminished presence of waters influenced by sea ice melt and the higher contributions from warmer waters during the 2017 cruise.

Despite the lower contributions from low-salinity melt waters, all seven transects during SKQ201712S still displayed stratified conditions (Figure 9). However, most profiles lacked the steep pycnoclines that characterized SKQ201612S and there were noticeable lateral differences in the distribution and spacing of isopycnals along the transects. Slightly more buoyant waters ($_{t} < 24$ kg m^{-3}) characterized the offshore sections of several transects in the northeast region of the study area (transects 1, 3, 4, 5) consistent with some influence from melt water. In transects from the southwestern region of the study area, especially transect 7 (DBO4 line) and to a lesser degree transect 6, low density surface waters coincided with near-shore locations. Virtually all deeper waters were characterized by $_{t}$ values between 25.5 and 26.0 kg m^{-3}. The major exception was transect 5 across Barrow Canyon (DBO5 line), which was occupied following the period of upwelling-favorable winds and displayed high-density waters ($_{t} > 26.0$ kg m^{-3}) throughout the deeper sections of the water column and along the southern flank of the canyon. Following the period of easterly wind forcing between August 12 and 17, 2017, isopycnals along this section of the canyon shifted from a down- to upward-tilting direction. Furthermore, high density waters reached the surface at the southernmost station of transect 5. Both of these observations are clear evidence of significant upwelling (Pickart et al., 2019) after this wind event (Fig. 2b). A more muted response to upwelling was evident when comparing density distributions off Wainwright before (transect 2) and after (transect 6) the wind event. In this case, the offshore extension of warmer temperatures in surface waters and the slight inshore shoaling of isopycnals along transect 6 compared to transect 2 were both consistent with the upwelling-favorable wind forcing. The difference in the magnitude of change between the two transects illustrate the sensitivity of Barrow Canyon to wind forcing relative to other inner shelf locations (e.g., Pickart et al., 2013; 2019). Overall, the densities of surface and mid-depth waters in SKQ201712S were greater than those in SKQ201612S, reflecting the importance of more buoyant waters derived from sea ice melt in September 2016 cruise (Table 1). Bottom waters showed comparable density averages during both cruises, but the higher variability in $_{t}$ exhibited during SKQ201712S reflects the presence of multiple water masses in the deeper water column in this cruise relative to SKQ201612S.

POC distributions superimposed on the density profiles (Fig. 9) showed for the most part low concentrations (< 5 mmol m^{-3}) in surface waters along the seven SKQ201712S transects. The major exceptions were inshore regions of transects occupied following the upwelling wind event (e.g., transects 5, 6 and 7). Samples from depths around the pycnocline ($24.5 <$ $_{t} < 25.5$ kg m^{-3}) displayed intermediate POC values (5 to 10 mmol m^{-3}), with a few instances of higher concentrations approaching 20 mmol m^{-3}. High-density ($_t$ > 25.5 kg m^{-3}) bottom waters generally displayed higher POC concentrations (> 10 mmol m^{-3}), although in some locations (e.g., transect 7) deep-water POC concentrations were significantly lower (5 mmol m^{-3}). Comparison of POC distributions prior and following the wind event (i.e. transects 1 vs. 5 and 2 vs. 6) showed marked increases in POC concentrations at various depths and density ranges, but increases were most noticeable along the nearshore sections off Barrow Canyon and Wainwright.

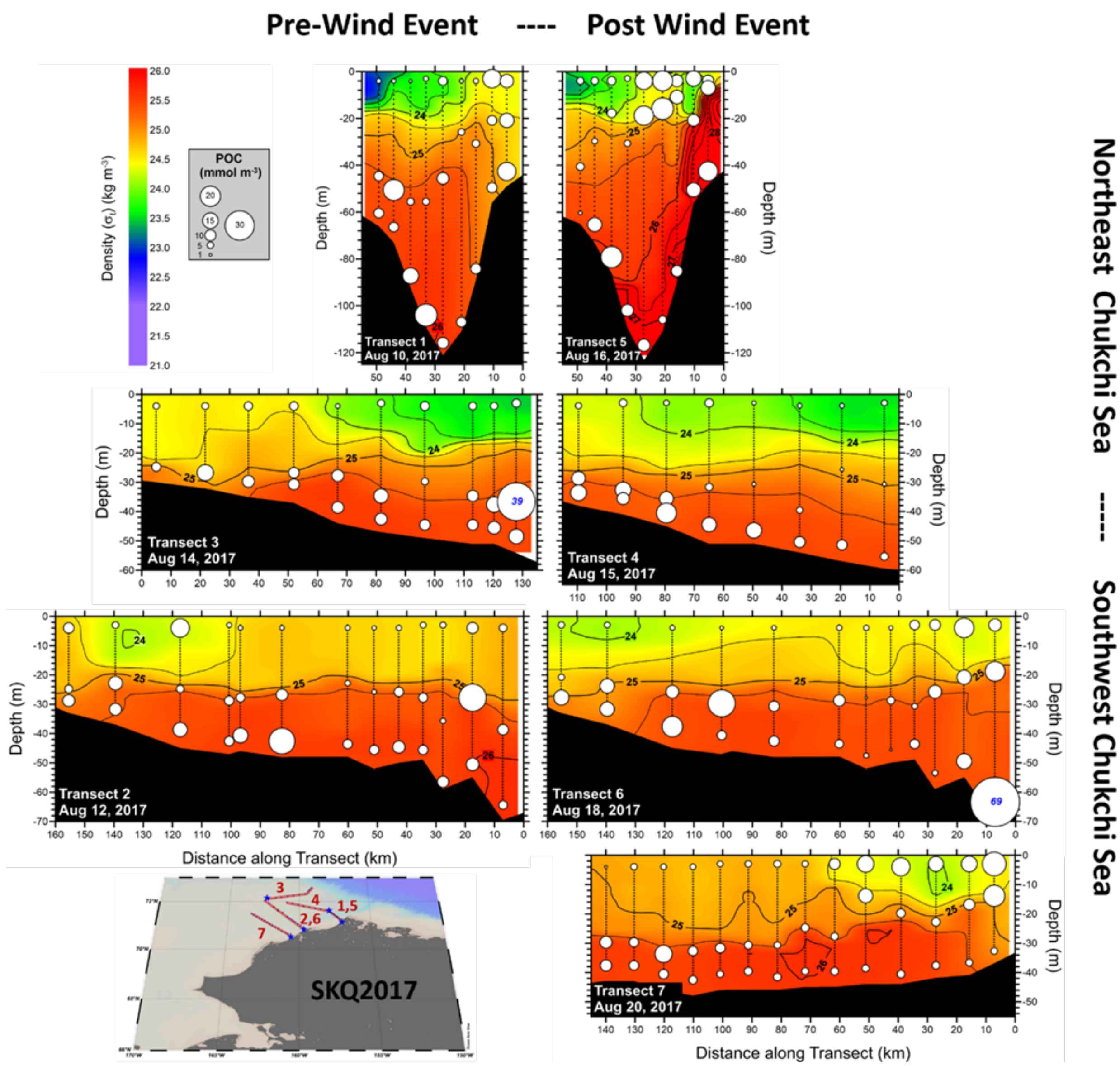

Figure 9. Distributions of density ($_{t}$; kg m^{-3}) throughout the water column and particulate organic matter concentrations (POC; M) from individual samples collected across the seven hydrographic transects completed during SKQ201712S. Note that the start of each transect is identified by a blue star in the map insert. The cross-section contour plots are based on binned downcast data collected at each CTD station indicated by dotted lines in each transect. The bubble plots showing POC concentrations are superimposed on the contour maps to identify the location of each individual sample.

The buildup of POC in surface waters at these locations was consistent with enhanced biomass following the period of upwelling winds, especially along the southern flank of Barrow Canyon. In the case of transect 6, we also measured a major increase in POC directly above the seabed at the most inshore station. Overall, despite the high variability, samples from the mid-depth and bottom regions of the water column during SKQ201712S displayed higher POC concentrations than those from SKQ201612S, highlighting contrasts in the overall abundance of POM during these two periods (Table 1).

Contour plots of Chl Fl signals along all seven transects revealed the presence of SCM that varied in intensity and location within and among transects (Figure 10).

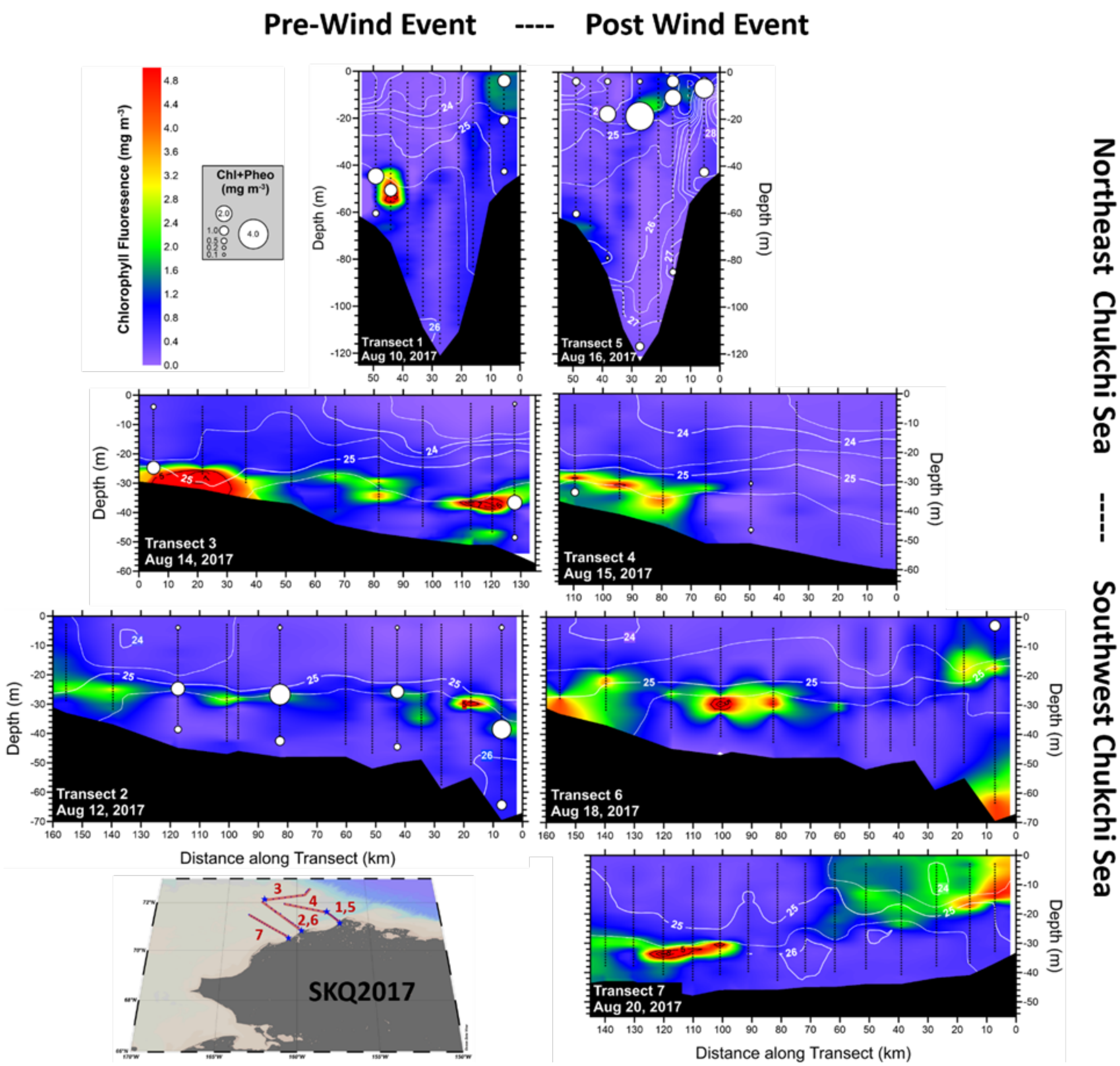

Figure 10. Distributions of chlorophyll fluorescence sensor measurements (Chl Fl; mg m^{-3}) throughout the water column and combined photosynthetic pigment concentrations – chlorophyll and pheophytin (Chl+Pheo; mg m^{-3}) – from individual samples collected across the seven hydrographic transects completed during SKQ201712S. Note that the start of each transect is identified by a blue star in the map insert. The cross-section contour plots are based on binned downcast data collected at each CTD station indicated by dotted lines in each transect. The bubble plots showing Chl+Pheo concentrations are superimposed

on the contour maps to identify the location of each individual sample.

Elevated Chl Fl values (> 2 mg m^{-3}) were generally measured at mid-depths associated with the bottom of the pycnocline ($_t$ ~ 25.5 kg m^{-3}) with a few locations displaying considerably higher values (> 4 mg m^{-3}). Overall, surface and deep waters consistently displayed low Chl Fl signals (< 0.5 mg m^{-3}) with a few exceptions.For example, surface inshore waters in transects 1, and especially transects 5, 6 and 7, which were occupied following the upwelling wind event displayed elevated Chl Fl values (1 to 3 mg m^{-3}). In addition, deep waters above the seabed displayed elevated Chl Fl signals at a few locations, including the region around Hannah Shoal (start of transect 3) and the inshore regions along transect 6, both of which also displayed moderate to very high POC concentrations. Combined pigment analyses (Chl+Pheo) from selected water samples displayed general agreement with the Chl Fl signals and suggest that the trends in the latter reflected the distribution of photosynthetic biomass rather than interferences from other potential sources of fluorescence. Overall, as was the case for POC, the Chl Fl values from samples collected during SKQ201712S from the mid-depth and bottom regions of the water column were somewhat higher than those collected from the same depth ranges during SKQ201612S (Table 1), likely reflecting differences in phytoplankton standing stocks in different water masses.

Figure 11 illustrates the particle beam attenuation characteristics of the water columns across all seven SKQ201712S transects and shows superimposed SPM concentrations from individual water samples. As was the case for the previous cruise, virtually all surface to mid-depth waters (23 < $_t$ < 25.5 kg m^{-3}) above or near the pycnocline in 2017 were characterized by very low c_p values (< 0.2 m^{-1}) and low SPM concentrations (< 3 g m^{-3}). The major exceptions were the inshore waters along the Barrow Canyon transects (transects 1 and 5) and the nearshore waters sampled along transects 6 and 7 following the upwelling wind event. In contrast, high-density ($_t$ > 25.5 kg m^{-3}) bottom waters displayed markedly elevated c_p values and SPM concentrations that ranged from 1 to 3 m^{-1} and 5 to 15 g m^{-3}, with the deep regions along the inshore station of transect 6 exhibiting very high values of c_p (> 3 m^{-1}) and SPM (27 g m^{-3}). While the overall extent and intensity of the particle-rich bottom waters differed between the two cruises (see Figs. 7 and 11), they both highlight the predominance of turbid conditions in bottom waters throughout much of the Chukchi shelf during the open water period. The ranges and overall averages of c_p and SPM during SKQ201712S were generally higher to those during SKQ201612S, especially in samples from the mid-depth and deeper regions of the water column (Table 1), consistent with comparable contrasts in other variables.

As was the case for SKQ201612S, during SKQ201712S we completed several CTD casts close to local noon when surface PAR (500 to 1000 Ein cm^{-2} s^{-1}) was at a maximum (Figure 12). These plots show steep light attenuation conditions were also prevalent during the August 2017 cruise, with some cases, such as stations 81 and 64, where the 1% PAR level corresponded to depths just below the pycnocline. Compared to the profiles obtained during September of 2016 (Fig. 7), the profiles obtained during August of 2017 showed steeper light attenuation conditions, especially following the upwelling-favorable wind event.

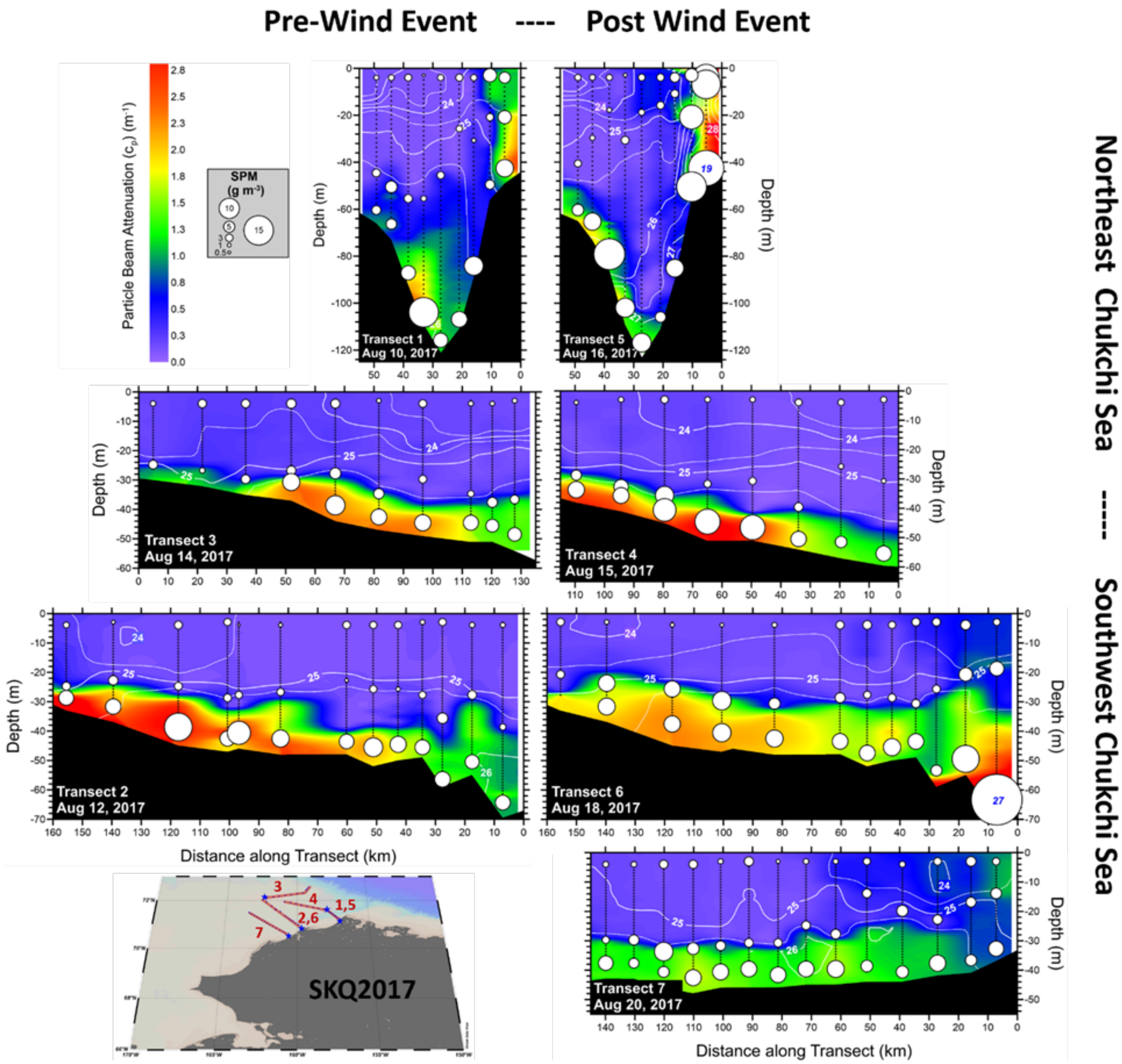

Figure 11. Distributions of particle beam attenuations sensor measurements (c_p; m^{-1}) throughout the water column and combined suspended particulate matter concentrations (SPM; g m^{-3}) from individual samples collected across the seven hydrographic transects completed during SKQ201712S. Note that the

start of each transect is identified by a blue star in the map insert. The cross-section contour plots are based on binned downcast data collected at each CTD station indicated by dotted lines in each transect. The bubble plots showing SPM concentrations are superimposed on the contour maps to identify the location of each individual sample.

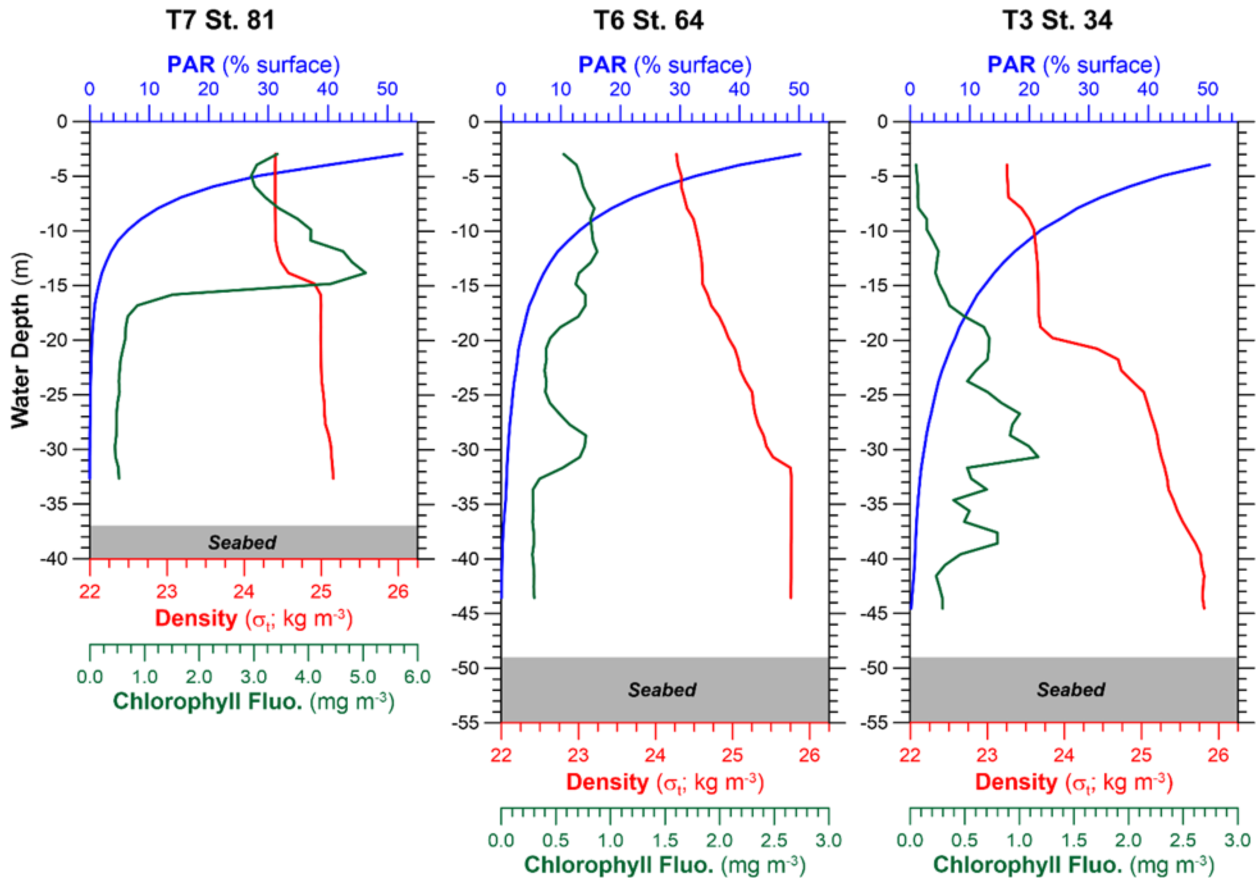

Figure 12. Profiles from selected hydrographic stations identified by transect (T#) and CTD station (St.#) numbers (see Figure 1) occupied near local mid-day during SKQ201712S. Local date/time occupation of these hydrographic stations is as follows: T3 St.34, August 14, 2017 at 12:25; T6 St.64, August 18, 2017 at 12:41; T7 St.81, August 20, 2017 at 11:19. The figures show depth profiles of density ($_t$; kg m^{-3}), chlorophyll fluorescence (mg m^{-3}) and photosynthetically active radiation (PAR; Ein cm^{-2} s^{-1}) measurements calculated as a percent of surface PAR.

4.2.3 Comparison with previous observations

The overall summaries of the different measurements carried out during SKQ201612S and SKQ201712S presented in Table 1 provide the opportunity to compare these data to those from previous studies of the same region. For example, temperature and salinity differences between the two cruises were especially notable in surface and mid-depth samples (Table 1), where warmer and saltier values characterized the late summer in 2017 relative to 2016. Similar compositional contrasts were measured throughout the Chukchi Shelf by Danielson and co-workers (2017) during two consecutive late seasons (Aug-Sep) in 2012 and 2013, highlighting the inter-annual variations in regional circulation and water mass distributions of this inflow shelf system. Depth-related density differences (e.g., Figs. 4 and 9) summarized by the $_{t}$ averages in Table 1 were consistent with previous studies (e.g., Danielson et al. 2017; Weingartner et al. 2017, Martini et al., 2016), which highlighted the impacts of water column stratification on dissolved nutrients and phytoplankton biomass distributions.

Our measurements of Chl Fl distributions during the 2016 and 2017 cruises (Table 1) were comparable to those measured in 2012 and 2013 by Danielson and co-workers (2017), who showed chlorophyll concentrations in surface waters north of Pt. Hope ranged between 0.2 to 0.5 mg m^{-3} in the region around Hannah Shoal and 0.6 to 1.0 mg m^{-3} in more inshore waters. Furthermore, both the overall ranges (Table 1) and depth distribution of Chl Fl in our study were comparable to previous measurements by Weingartner and co-workers (2017), who showed transects near Hannah Shoal in 2012 with a well-defined SCM (2 to 10 mg m^{-3}) located immediately below pycnocline depths. Martini et al. (2016) showed similar ranges of chlorophyll concentrations at the SCM in the northeast region around Hannah Shoal during cruises in Aug-Sep 2013. As was the case for our study (e.g. Figs. 7 and 12), these authors detected the SCM in a region of the water column that was below the mean pycnocline depth but above the mean euphotic depth as defined by the 1% PAR level. The overall agreement with previous measurements indicate the POM distributions and characteristics we measured during the 2016 and 2017 cruises are representative of late season conditions in this region of the Chukchi Shelf.

Our measurements of POC and photosynthetic pigment (Chl+Pheo) concentrations during both SKQ201612S and SKQ201712S (Table 1) can be compared to previous studies investigating the seasonal evolution of phytoplankton productivity during the spring-summer period along the NE Chukchi Shelf . For example, studies conducted in June-July of 2010 showed markedly elevated chlorophyll ($>$ 30 mg m^{-3}) and POC ($>$ 60 mmol m^{-3}) concentrations in surface and subsurface waters from the central and NE Chukchi Sea that were much higher than those in this study (Table 1) and consistent with under-ice and ice-edge blooms in the spring (Arrigo et al., 2014; Brown et al., 2015; Lowry et al., 2015). Measurements conducted during the 2002 spring (May-June) and summer (July-August) open-water period along the NE Chukchi Sea (e.g., Hill and Cota, 2005; Bates et al., 2005) showed POC concentrations that ranged from 2 to 40 mmol m^{-3} and chlorophyll concentrations that ranged from 0.2 to 6 mg m^{-3} along the regions around Hannah Shoal and Barrow Canyon. The highest values in both POC and chlorophyll were measured during the July-August period and were found in sub-surface regions of the water column at or below the pycnocline. Our measurements during the August-September period generally agree with these trends and show moderately elevated photosynthetic pigment and POC concentrations at the mid-depths (Table 1). The fact that these features are present through the late summer-early fall suggest the importance of wind-driven mixing of nutrient-rich waters in maintaining sub-surface productivity during the late open-water season (e.g., Martini et al., 2016; Stabeno et al., 2020; Nishino et al. 2020; Ardyna and Arrigo, 2020).

Finally, our observations of elevated c_p values and high SPM concentrations in bottom-waters throughout the Chukchi Shelf were consistent with data from Martini et al. (2016), who measured high turbidity in denser waters below the pycnocline along shelf-transects near Hannah Shoal in September 2013. Mooring-based measurements along the Beaufort Sea margin by Forest et al. (2013; 2015) showed high turbidity waters off the Mackenzie Shelf during the open water season (July-Aug) that were not correlated with Chl Fl and were consistent with periods of energetic and downwelling-favorable wind conditions at the shelf-break. Cross-margin transects in this region during the summer period showed high density ($_t$ > 25.5 kg m^{-3}) bottom waters with low transmissivity (consistent with c_p > 0.5 m^{-1}) originated in shallower regions of the shelf (e.g., Forest et al., 2007). Several reports of SPM concentrations in Chukchi Sea waters include observations by Moran et al. (2005), who reported slightly elevated SPM values (~ 0.5 – 1.0 g m^{-3}) in bottom waters along the shelf-break east of Hannah Shoal and Barrow Canyon during Spring of 2002, a period of intermediate productivity (Hill and Cota, 2005). Neukermans and co-workers (2014) measured c_p and SPM across the NE Chukchi shelf during the NASA ICESCAPE study in July 2011 and reported intermediate values (c_p ~ 0.5 to 1. 0 m^{-1}; SPM ~ 2 g m^{-3}) in bottom waters near Hannah Shoal under open water conditions, and markedly higher values (c_p ~ 1 to 2 m^{-1}; SPM ~ 8 g m^{-3}) north of Hannah Shoal in under-ice conditions. There were distinct differences in the Chl and POC distributions associated with these samples which, along with further studies of optical characterization (e.g., particle backscatter), point toward contrasts among particle sources and compositions within the Pacific Arctic waters (e.g., Neukermans et al., 2016; Reynolds et al., 2016).

5 Discussion

The spatial, temporal and depth-related trends in POM distributions presented above and summarized in Table 1 cannot be fully understood without careful consideration of hydrographic conditions during the two cruise periods. In the following sections, we examine water mass distributions across the northeast Chukchi Shelf and relate the concentrations and compositions of POM to the distinct distribution patterns and wind forcings experienced during the two late-summer periods.

5.1 Late season hydrographic trends

We can investigate the distributions of water masses across the Chukchi Shelf during the two late season cruises by plotting temperature and salinity compositions for the different stations and transects (Figure 13). In these graphs we chose to highlight the compositions of distinct water masses based on the temperature and salinity signatures defined by Danielson and co-workers (2017), who conducted hydrographic surveys of this region during the late summer. For example, during SKQ201612S (Fig. 13 a, b), a large fraction of surface waters in this region of the Chukchi Shelf is made up of low-density (22 > $_t$ > 24 kg m^{-3}) waters with salinity-temperature signatures consistent with a Melt Water (MW) source. Much of this MW is quite cold (-1 C) and relative fresh (salinity < 28), which is consistent with inputs from recently melted sea ice along offshore sections of transects 3, 4, 5 and 8 around Hannah Shoal, where we encountered the ice pack. In transects 2, 6, 7 further to the west, MW waters are warmer (> 0 C) and saltier (> 28) and likely influenced by mixing with other water masses. Intermediate density (24 > $_t$ > 25.5 kg m^{-3}) Bering/Chukchi Summer Water (BCSW) and Bering/Chukchi Winter Water (BCWW) occupy the mid-depths across the study area and contribute to the strong pycnoclines observed during SKQ201612S. Relatively warm (2 to 5 C) BCSW occupies mid-depths along transects 2, 6, 7, whereas low salinity (30 to 31.5) BCWW occupies the mid-depth sections of the water column further to the northeast along transects 3, 4, 8). The deeper sections of the water column during SKQ201612S are occupied by high-density ($_t$ > 25.5 kg m^{-3}) waters that constitute the bottom mixed layer and are made up of BCWW and BCSW, with marked spatial differences among and within transects (Fig. 13 a, b).

The salinity-temperature plots for SKQ201712S (Figure 13 c, d) illustrate quite different conditions from those of SKQ201612S, reflecting the occupation of stations inshore of the 30-mile distance and the diminished influence of sea-ice melt during the 2017 cruise. As shown in these graphs, BCSW is the major water mass throughout much of study area for SKQ201712S, with large swaths of all transects being occupied by these intermediate-density (24 > $_t$ > 25.5 kg m^{-3}) modified summer waters. Lower-density (22 > $_t$ > 24 kg m^{-3}) MW is found in some sections of transects 1, 3, 4, whereas we find intermediate-density (24 > $_t$ > 25 kg m^{-3}) ACW with temperatures above 7 C in nearshore sections of transects 1, 5, 6, 7. The deeper sections of the water column are occupied primarily by high-density ($_t$ > 25.5 kg m^{-3}) BCSW and BCWW, with the latter being found along transects 1, 3, 4, 5. The other major water mass observed during SKQ201712S is high-salinity (> 33) dense (> 26 kg m^{-3}) AtlW, which is found along the deeper part and southern sections of transect 5 following the upwelling event.

1. **b)**

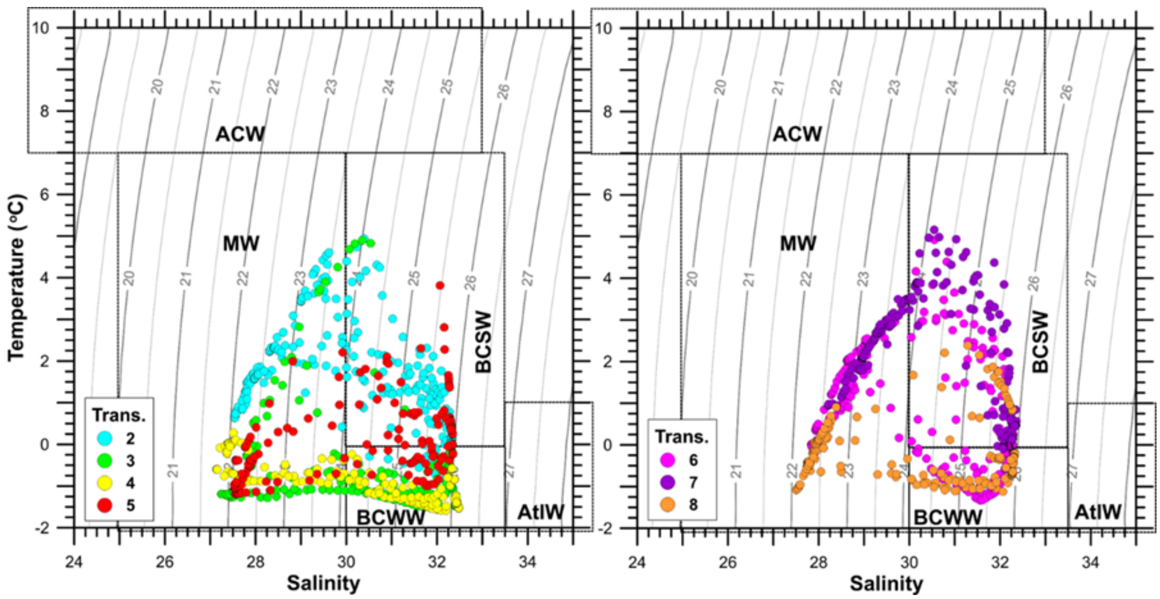

c) d)

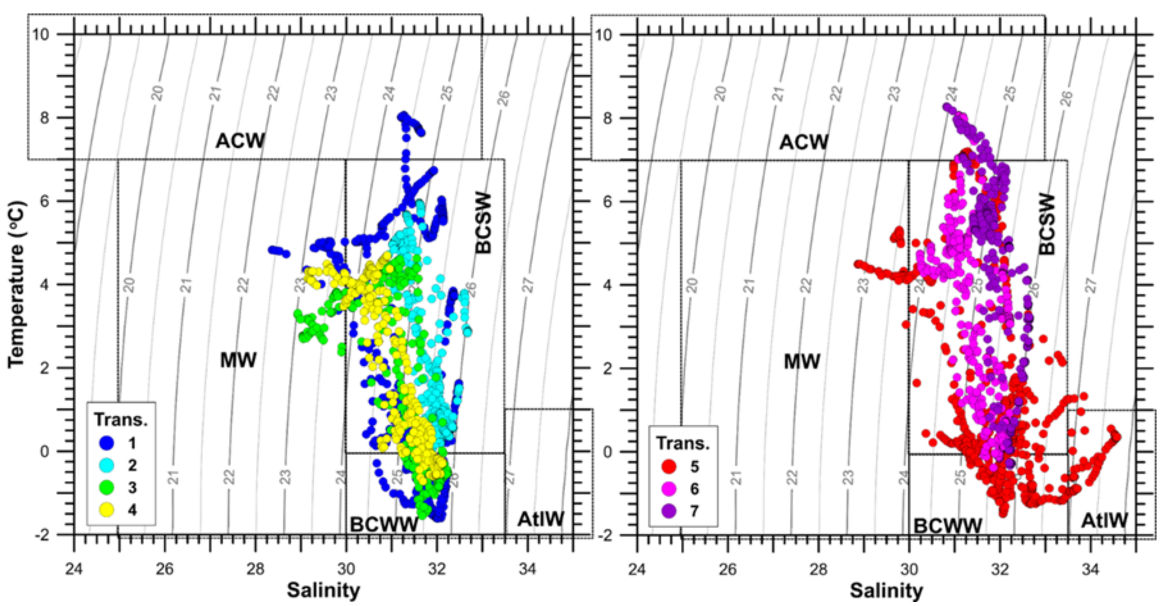

Figure 13. Temperature-Salinity plots summarizing hydrographic compositions measured during SKQ201612S before and after the Sep 17-20, 2016 downwelling-favorable wind event (a and b, respectively) and during SKQ201712S before and after the August 12-17, 2017 upwelling-favorable wind (c and d, respectively). The transects occupied during each period are identified by the different colors. The plots also include the temperature-salinity ranges

for different regional water masses based on the data from Danielson et al., 2017. The water masses shown include Alaska Coastal Water (ACW), Melt Water (MW), Bering-Chukchi Summer Water (BCSW), Bering-Chukchi Winter Water (BCWW), and Atlantic Water (AtlW). Also shown are lines of equal density ($_t$; kg m^{-3}) for the temperature and salinity ranges in each graph.

The spatial trends in water mass distributions, which are illustrated in Figures 2S and 3S, reflect the regional circulation in this area of the Chukchi Shelf (e.g. Fig. 1a; Danielson et al., 2017; Weingartner et al., 2017; Pacini et al., 2019; Okkonen et al. 2019) and highlight the contrasts between the two late-season cruises. For example, in SKQ201612S, most of the top 20 m of the water column through the study area is occupied by MW, which overlies denser BCWW and BCSW and results in the strong stratification conditions observed (Fig. 2S). Notably, MW overlies nutrient-rich remnant winter water (BCWW) in many of sections south and east of Hannah Shoal (e.g., transects 3, 4, 8), whereas nutrient-poor, modified water (BCSW) is found in regions west of Hannah Shoal (e.g., transects 2, 6 and 7). In contrast, during SKQ201712S, highly modified, nutrient-poor BCSW occupies much of the water column throughout the study area, including surface waters across transects to the south, west and directly over the Hannah Shoal region (Fig. 3S). The ubiquitous extent of BCSW combined with the restricted distribution of more buoyant water masses (e.g., MW and ACW) helps to explain the markedly lower degree of water column stratification that characterize SKQ201712S. Furthermore, unlike SKQ201612S, the distribution of nutrient-rich BCWW across the northeast Chukchi Shelf during SKQ201712S is restricted to the deepest regions of the water column east of Hannah Shoal and is overlain by modified BCSW. Figure 3S shows multiple water masses across Barrow Canyon, highlighting the more complex circulation associated with this feature and its response to wind-driven upwelling (e.g., Pickart et al. 2019; Okkonen et al., 2019).

As illustrated by Figures S2 and S3, the hydrographic responses to wind forcing on the shelf itself are more muted but display patterns consistent with previous observations (e.g., Weingartner et al., 2017b; Pickart et al., 2019). For example, after the downwelling-favorable wind-event in SKQ201612S we see changes that are consistent with an enhanced presence of BCWW in the offshore region west of Wainwright (see transect 6 vs. 2) and a deepening of the mixed layer across the southern flank of Hannah Shoal (offshore region of transect 8 vs. 3). Given the strong westerly winds measured in the period (Sep 16-21, 2016) between the repeated transects, we infer that enhanced advection and mixing likely contribute to the changes observed. In the case of SKQ201712S, the main effect of the strong easterly winds (Aug 12-15, 2017) is seen across Barrow Canyon, with the occurrence of AtlW across the southern flank of the Canyon and the offshore displacement of ACW across the surface (Fig. 3S), both consistent with the responsiveness of the canyon to upwelling-favorable wind forcing (e.g., Pickart et al., 2019; Pisareva et al., 2019). The offshore extension of ACW following the easterly wind-period is the main effect of upwelling across the shallow shelf regions to the west of Barrow Canyon (e.g., transect 6 vs. transect 2; transect

7).

Overall, the observed contrasts in water mass distributions reflect inter-annual differences in oceanographic conditions in the study area as well as contrasts in the spatial coverage of Chukchi Shelf afforded during each cruise. Furthermore, there are noticeable differences in the composition and structure of the water column across the northeast Chukchi Shelf in response to distinct wind forcings. The differences among transects occupied prior and following wind events reflect their distinct nature (i.e. downwelling- vs. upwelling-favorable) and variable magnitude. However, it is also clear that location (e.g., deeper Barrow Canyon vs. shallower Chukchi Shelf) relative to key geographical features (e.g., shoreline, Hannah Shoal) also influence the structure of the water column along any given transect. Understanding these contrasts and controls on water column POM is critical to evaluate the biogeochemical responses of this region of the Pacific Arctic during the prolonged open-water period.

5.2 Water mass-POM distributions along Chukchi Shelf

In order to decipher the spatial and temporal patterns in POM distributions, we chose to evaluate compositional trends in the context of hydrographic conditions and water mass distributions. Hence, we use temperature-salinity class plots of Chl Fl to investigate density-related trends in chlorophyll distributions among water masses (Figure 14).

1. **b)**

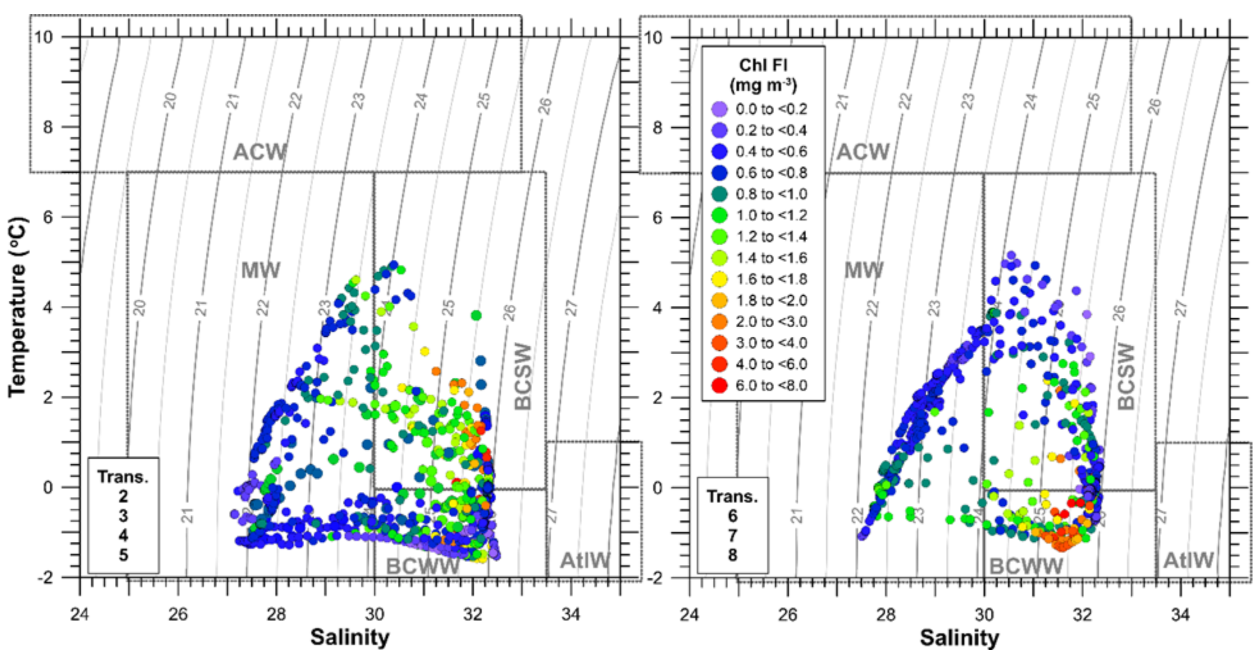

c) d)

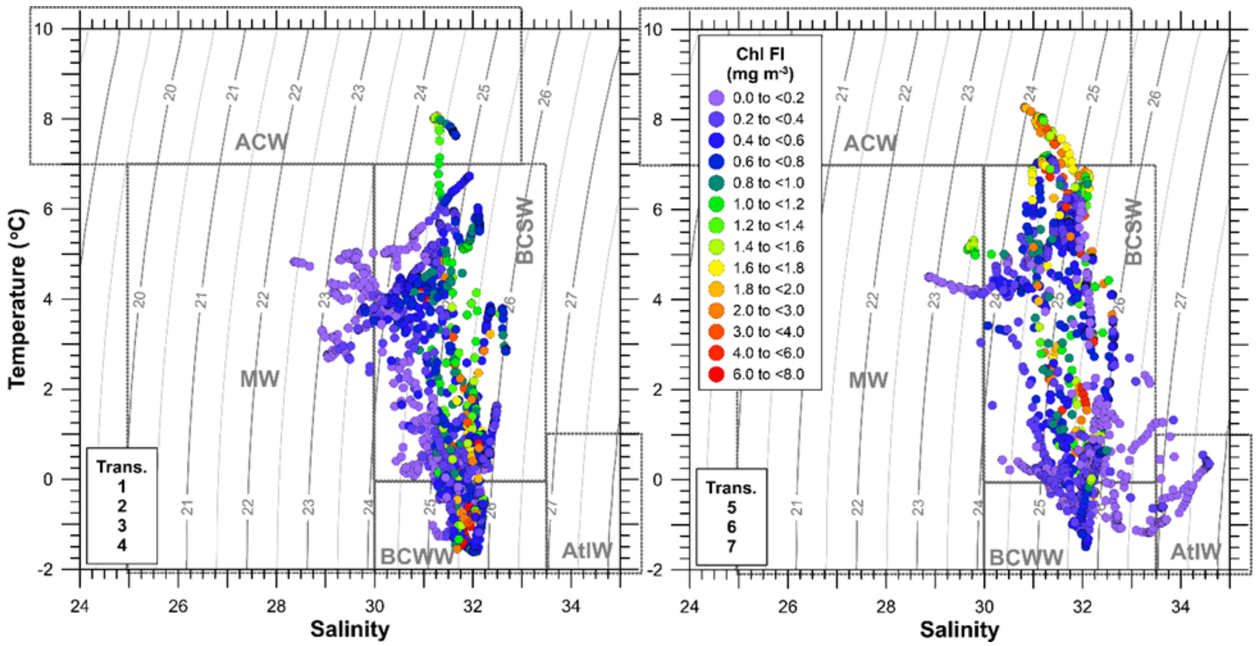

Figure 14. Chlorophyll fluorescence (Chl Fl; mg m^{-3}) sensor data plotted in temperature-salinity graphs for stations occupied during SKQ201612S before and after the Sep 17-20, 2016 downwelling-favorable wind event (a and b, respectively) and during SKQ201712S before and after the August 12-17, 2017 upwelling-favorable wind (c and d, respectively). The plots include the temperature-salinity ranges for different regional water masses based on the data from Danielson et al., 2017. The water masses shown include Alaska Coastal Water (ACW), Melt Water (MW), Bering-Chukchi Summer Water (BCSW), Bering-Chukchi Winter Water (BCWW), and Atlantic Water (AtlW). Also shown are lines of equal density ($_t$; kg m^{-3}) for the temperature and salinity ranges in each graph.

For example, during SKQ201612S, we generally find low to moderate Chl Fl values (0.8 to 1.4 mg m^{-3}) before the wind event of Sep 17-20, 2016 in all three water masses. In fact, prior to the wind event, the high Chl Fl values (> 1.8 mg m^{-3}) that define the SCM are most predominant in higher-density BCSW (e.g., transect 2; Fig. 5) rather than in BCWW (e.g., transect 3; Fig. 5). Following the period of sustained downwelling winds, the high Chl Fl values shift to BCWW (Fig. 14b), especially in the region west of Wainwright (i.e., transect 6; Fig. 5). This trend, illustrated by the contrast between transects 2 and 6, indicates a deepening of the SCM due to mixing and advection of nutrient-rich BCWW in this region of the shelf (e.g., Fig. 2S). The SKQ201712S data show that prior to the upwelling wind event in Aug 12-17 (2017), peaks in Chl Fl associated with the SCM occur in high density (25 > $_t$ > 26 kg m^{-3}) waters in both BCWW and BCSW (Fig. 14c). Following the period of upwelling winds, higher Chl Fl values are observed in lower density BCSW and ACW (Fig. 14d), consistent with a phytoplankton productivity response due nutrient mixing into upper parts of the water column along nearshore locations (Fig. 3S).

Similar temperature-salinity plots of c_p (Figure 15) reveal distinct trends in overall particle distributions that indicate chlorophyll-depleted particles are for the most part responsible for the elevated turbidity levels (c_p > 1 m^{-1}) found in the densest ($_t$ ~ 26 kg m^{-3}) waters, including BCSW, BCWW and AtlW. The fact that the high c_p and SPM values (Figs. 6 and 11) coincide with dense bottom waters during both cruises (Figs. 15 a-d) is a strong indication that interactions with the seabed through resuspension and/or advection of pigment-depleted, mineral-rich particles contribute to the observed particle distributions along the NE Chukchi Shelf. The major exception are samples from the warm (~8 °C), intermediate density (24 > $_t$ > 25 kg m^{-3}) ACW that were measured in the nearshore section off Barrow Canyon (transect 1; Fig.11) during SKQ201712S prior to the wind event (Fig. 15c). It is likely that mineral-rich particles entrained within the ACW contribute to the elevated turbidity readings. In contrast, following the upwelling-wind event in 2017 (Fig. 3S), wind-induced phytoplankton production leads to elevated Chl Fl (Fig. 14d) but relatively low c_p values (Fig. 15d) in samples from ACW.

The compositions of individual samples can also be evaluated in the context of different water masses in the same way we assess the particle-related optical properties above (e.g., Chl Fl and c_p). For example, Figure 16 illustrates POC concentrations in temperature-salinity graphs and shows that despite the reduced number of individual samples, there are statistically-significant differences among water masses measured in this study. Tables 2 and 3 provide summaries of the concentration data from individual samples for different water masses binned into density ranges and cruise periods prior/following the wind events. From both Figure 16 and Table2, it is apparent that in SKQ201612S, moderate to elevated POC concentrations (8 mmol m^{-3}) coincide with cool, low density (21 > $_t$ > 23 kg m^{-3}) MW whereas the higher-salinity, higher density MW samples have lower POC concentrations (Fig. 16 a, b). All these samples are characterized by low Chl Fl signals, low c_p values, and low to moderate Chl+Pheo and SPM concentrations (Table 2). In contrast, the warmer and saltier MW samples measured during SKQ201712S are characterized by lower POC and lower Chl Fl values (Table 3). Overall, these trends suggest moderately elevated levels of phytoplankton biomass associated with surface waters affected by recently melted sea ice, which we encountered primarily in SKQ201612S (e.g., Fig. 2S). The contrasting distributions between the two cruises likely reflect higher contributions from phytoplankton to suspended particles in recently formed, colder and fresher MW in SKQ201612S relative to the warmer MW encountered in SKQ201712S (Fig. 3S).

1. **b)**

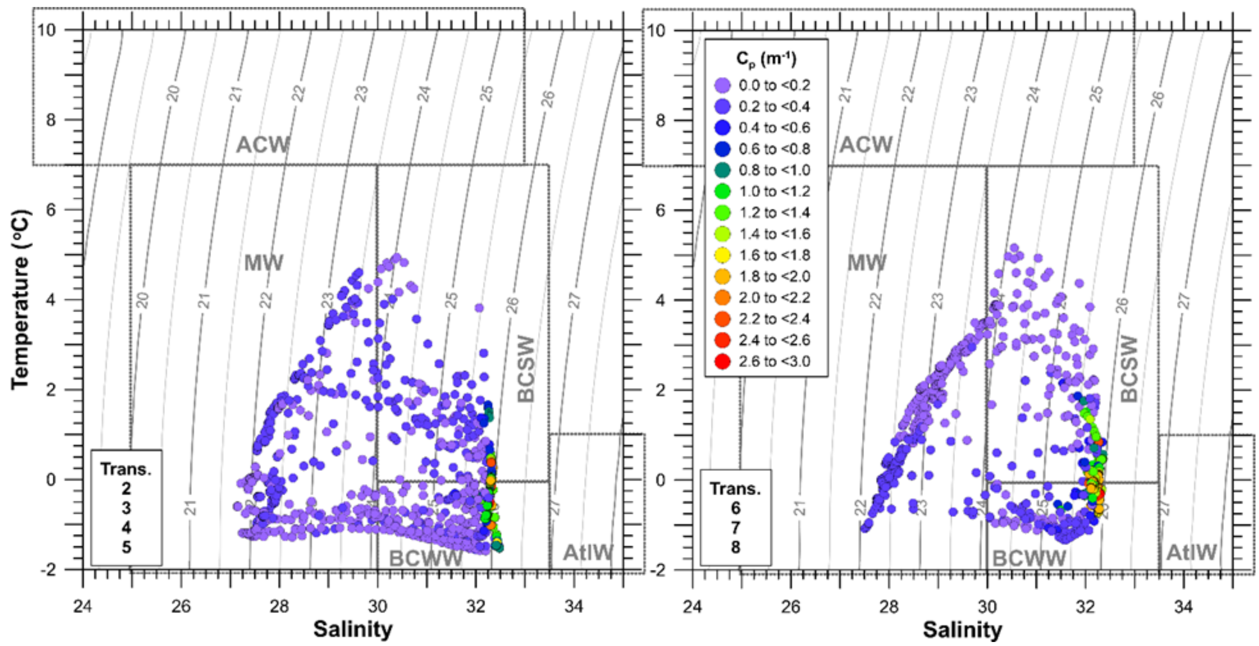

1. **d)**

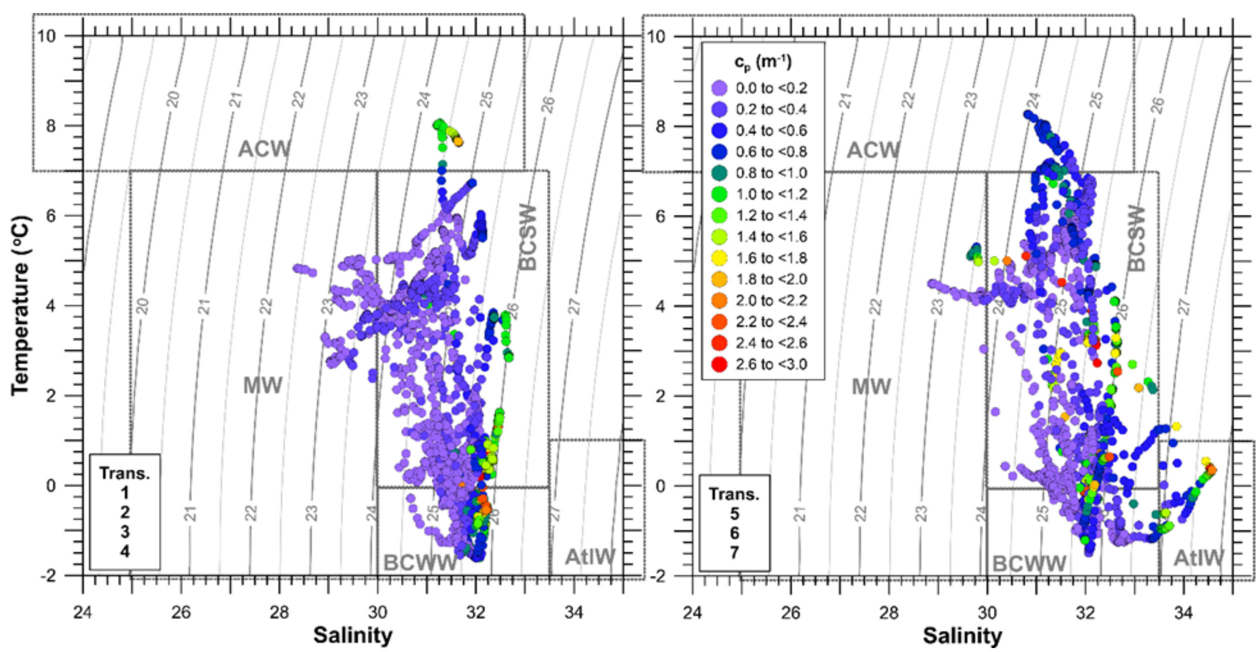

Figure 15. Particle beam attenuation (c_p; m^{-1}) sensor data plotted in temperature-salinity graphs for stations occupied during SKQ201612S before and after the Sep 17-20, 2016 downwelling-favorable wind event (a and b,

respectively) and during SKQ201712S before and after the August 12-17, 2017 upwelling-favorable wind (c and d, respectively). The plots include the temperature-salinity ranges for different regional water masses based on the data from Danielson et al., 2017. The water masses shown include Alaska Coastal Water (ACW), Melt Water (MW), Bering-Chukchi Summer Water (BCSW), Bering-Chukchi Winter Water (BCWW), and Atlantic Water (AtlW). Also shown are lines of equal density ($_{t}$; kg m^{-3}) for the temperature and salinity ranges in each graph.

a) b)

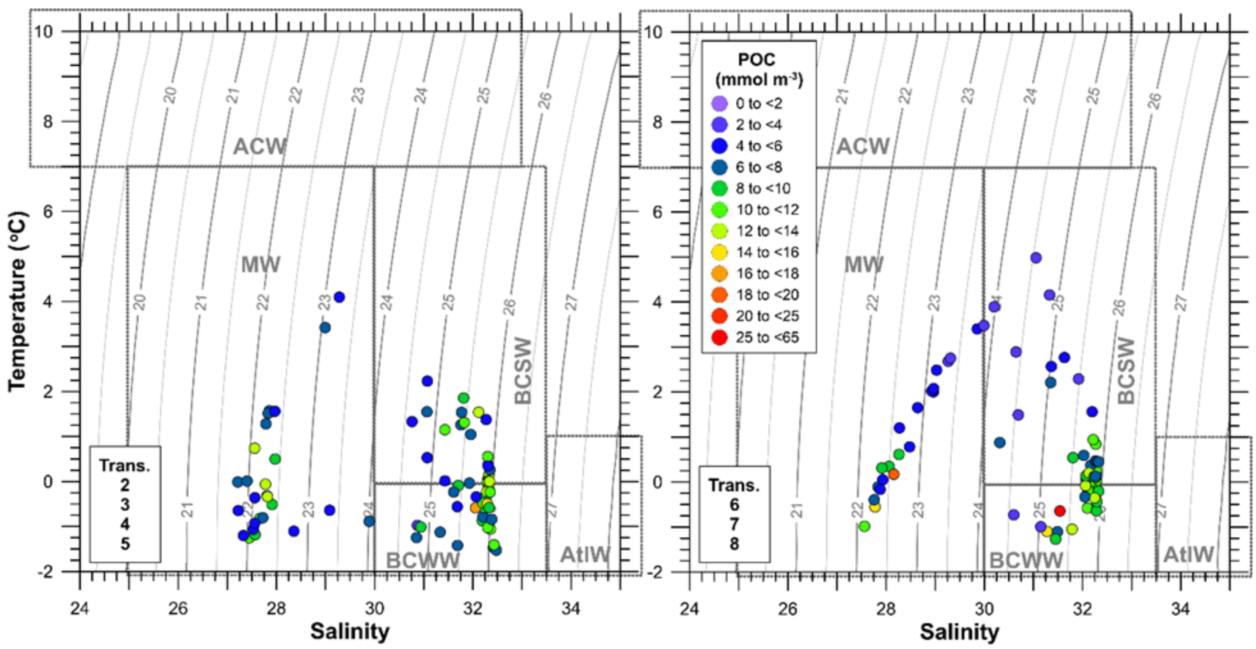

c) d)

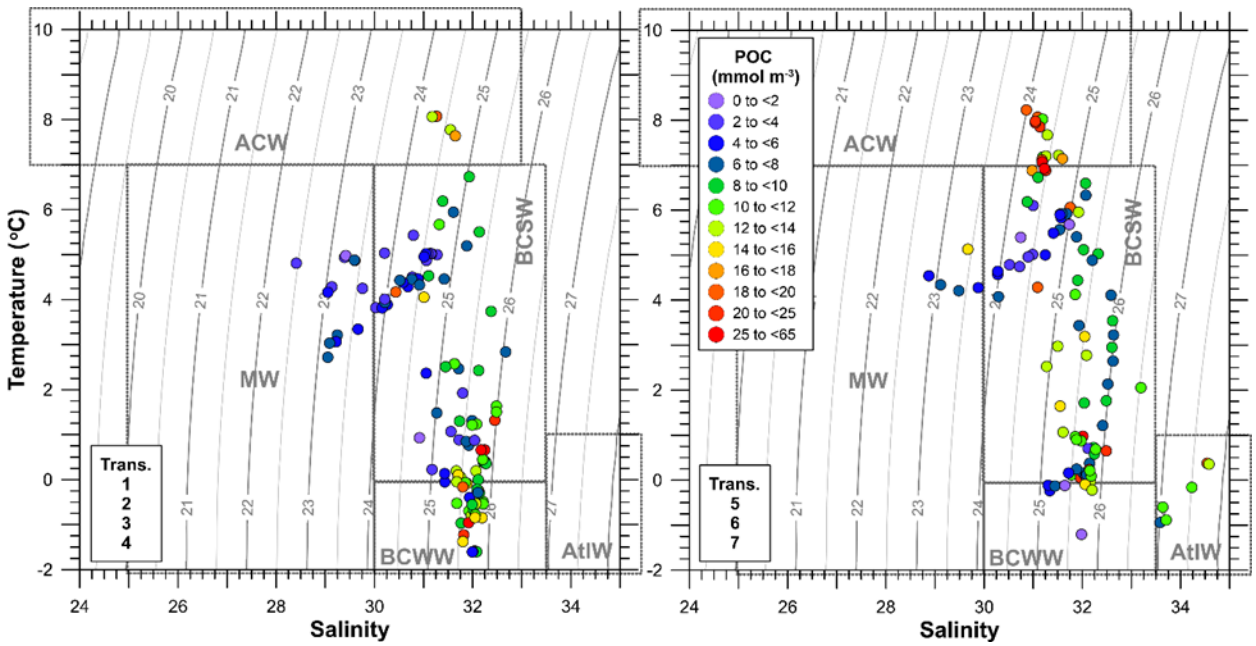

Figure 16. Particulate organic carbon (POC; mmol m^{-3}) concentrations from individual water samples plotted in temperature-salinity graphs for stations occupied during SKQ201612S before and after the Sep 17-20, 2016 downwelling-favorable wind event (a and b, respectively) and during SKQ201712S before and after the August 12-17, 2017 upwelling-favorable wind (c and d, respectively). The plots include the temperature-salinity ranges for different regional water masses based on the data from Danielson et al., 2017. The water masses shown include Alaska Coastal Water (ACW), Melt Water (MW), Bering-Chukchi Summer Water (BCSW), Bering-Chukchi Winter Water (BCWW), and Atlantic Water (AtlW). Also shown are lines of equal density ($_t$; kg m^{-3}) for the temperature and salinity ranges in each graph.

During SKQ201712S, moderate to high POC concentrations (12 mmol m^{-3}) in surface waters are measured in samples from ACW, especially following the wind event (Fig. 16 c, d) when high Chl Fl and low- to moderate c_p values are also measured (Table 3). In contrast to MW, ACW samples in SKQ201712S have significantly elevated SPM and Chl+Pheo concentrations that coincide with the high POC concentrations and high Chl Fl and c_p values. Unlike MW samples, there are significant differences in Chl+Pheo and SPM concentrations (as well as Chl Fl and c_p signals) before and after the August 12-17, 2017 period (Table 3), that are consistent with an increase in phytoplankton biomass and a decrease in mineral-rich particles following the upwelling-favorable wind event. Overall, the statistically distinct compositions of ACW and MW samples reflect clear differences in both overall particle abundance and provenance between these two water masses that occupy surface sections of the northeast Chukchi Shelf during the late, open-water season (Fig. 2S and 3S).

Samples from BCSW and BCWW, which occupy the majority of the mid-depth and bottom regions of the water column across the northeast Chukchi Shelf, display variable compositions that are strongly related to density (Tables 2 and 3). For example, in both SKQ201612S and SQK201712S, samples from low- to intermediate-density ($_{t}$ < 25.5 kg m^{-3}) BCSW are characterized by low to moderate POC concentrations (> 8 mmol m^{-3}), whereas the higher-density ($_{t}$ > 25.5 kg m^{-3}) samples display higher POC concentrations (>8 mmol m^{-3}) that in some cases exceed 20 mmol m^{-3} (Fig. 16). Samples from low density (23.5 > $_{t}$ > 24.5 kg m^{-3}) BCSW are characterized by low to intermediate Chl Fl values (0.3 to 1 mg m^{-3}), whereas those of intermediate density (24.5 > $_{t}$ > 25.5 kg m^{-3}) associated with the top of the pycnocline display significantly higher Chl Fl (1 to 2 mg m^{-3}) values (Tables 2 and 3). The combined pigment data, although sparse, show similar overall trends with moderately elevated Chl+Pheo concentrations that contribute to the SCM observed in transects from both cruises. Samples from both of these density ranges are characterized by relatively low c_p signals (0.1 to 0.5 m^{-1}) and low SPM concentrations (2 to 4 g m^{-3}), with samples from SKQ201712S (Table 3) displaying higher averages than samples from SKQ201612S (Table 2). Relative to their lower-density counterparts, higher-density (25.5 > $_{t}$ > 26.0 kg m^{-3}) BCSW samples from both cruises (Tables 2 and 3) have higher POC concentrations (9 to 12 mmol m^{-3}) and are characterized by comparable Chl Fl values (1 to 2 mg m^{-3}) and Chl+Pheo concentrations (1 to 2.5 mg m^{-3}) but significantly higher c_p values (~1.4 m^{-1}) and SPM concentrations (6 to 8 g m^{-3}). Notably, within this density range, BCSW samples with densities greater than 26.0 kg m^{-3} collected during SKQ201712S have lower Chl Fl and Chl+Pheo concentrations and higher POC, c_p and SPM values (Table 3).

In the case of BCWW, sample compositions from different density ranges display patterns that are similar to those from BCSW (Tables 2 and 3). For example, the few samples from low density (24 > $_{t}$ > 25.5 kg m^{-3}) BCWW measured in both SKQ201612S and SKQ201712S display low to intermediate POC concentrations (Fig. 16) that coincide with high Chl Fl and Chl+Pheo values and relatively low c_p and SPM concentrations (Tables 2 and 3). A major exception were samples collected following the upwelling wind event during SKQ201712S (Table 3), which display much lower POC (~ 4 mmol m^{-3}) and Chl Fl (0.4 mg m^{-3}) values than the rest of the samples in this density category (see below). As was the case for BCSW, samples from the higher-density range (24 > $_{t}$ > 25.5 kg m^{-3}) of BCWW in both cruises display higher POC concentrations (10-12 mmol m^{-3}) and Chl Fl values (2 to 5 mg m^{-3}) and high c_p values and SPM concentrations (Table 2), all consistent with particle-rich, high turbidity deeper waters.

The marked contrasts among samples from BCSW and BCWW are clear evidence of fundamental density-related differences in POM composition and provenance within these water masses, which help explain the overall patterns observed during both cruises. Furthermore, by examining in more detail the trends associated with the wind events in both SKQ201612S and SKQ201712S, we observe some significant contrasts among specific density ranges that suggest biogeochemical responses to the wind-forcing in sub-surface waters (Tables 2 and 3). For example, in SKQ201612S there are significant increases in Chl Fl, c_p, POC and SPM following the downwelling mixing event in samples from lower-density BCWW associated with pycnocline ($24 > {}_t > 25.5$ kg m^{-3}) waters (Table 2). A similar increase is not observed in the higher-density BCWW samples from deeper waters and, most significantly in samples from similar density-ranges of BCSW (Table 2). These observations suggest wind-driven mixing events of nutrient-rich, winter waters (BCWW) are likely to result in more noticeable biologic responses – i.e. increases in POM production – than in the nutrient-poor, modified summer waters (BCSW). In terms of responses to the upwelling-favorable wind event in SKQ201712S, there are no major contrasts in intermediate- and high-density BCSW and BCWW that provide evidence of a region-wide response to the wind event. However, we do see increases of Chl Fl, Chl+Pheo and POC in intermediate-density ($24.5 > {}_t > 25.5$ kg m^{-3}) BCSW samples from the Barrow Canyon transect following the wind event (e.g., transects 1 vs. 5; Figs. 9 and 10) that contribute to the overall trends seen in Table 3. Note that the high variability within these samples leads to lower statistical significance in the difference between before and after compositions. Our results indicate the response of BCSW to upwelling differs regionally and is consistent with the sensitivity of Barrow Canyon to this forcing (Pickart et al., 2013; 2019).

In the case of the contrasts among lower-density ($24 > {}_t > 25.5$ kg m^{-3}) BCWW samples during SKQ201712S, it is likely that the observed decreases in POC and Chl Fl are a result of our sampling of different locations before and after the wind event (Fig. 3S). Prior to the wind event, samples from this density range of BCWW originated primarily from the region north and east of Hannah Shoal (transects 3 and 4) and also from the offshore region of Barrow Canyon (transect 1; Figs. 9 and 10), the latter of which included several samples with elevated POC and Chl Fl signals. Following the wind event, the only samples from this specific water mass density range were collected from the offshore region of Barrow Canyon (transect 5), which lacked the localized maxima seen in transect 1. Hence, we conclude that the contrasts between BCWW samples evident in Table 3 are due to the fact that no samples of BCWW from the region around Hannah Shoal were collected during the period following the upwelling event (Fig. 3S) and that the high POM feature present in the north flank of Barrow Canyon in transect 1 was not found in transect 5.

It is clear that the elevated Chl Fl values (> 1 mg m^{-3}) that define the SCM are observed in samples from a range of densities and water masses (Tables 2 and 3). Although sparse, the combined pigment (Chl+Pheo) concentration data for the most part confirm the Chl Fl sample data and show that unlike POC, elevated photosynthetic pigment concentrations expand over a broader density range in both BCSW and BCWW. In contrast, c_p values, POC and SPM concentrations peak in the samples from higher-density BCSW and BCWW that occupy the deeper regions above the seabed. These observations suggest that different types of particles are present in the sub-surface regions of the water column during the late, open-water season in this region of the Chukchi Shelf. Particles in the intermediate-density, mid-depth waters appear to be enriched in photosynthetic pigments and contain materials with relatively low light-attenuation properties. In contrast, particles in the denser, deeper regions of the water column, while still containing measurable pigments, include materials that have much greater light-attenuation capacity. The distinct distribution and variable concentrations of these particle types across density ranges in both BCSW and BCWW are responsible for the patterns we observe and directly influence the overall profiles of POM measured in Chukchi Shelf waters.

5.3 Compositional characteristics and provenance of late-season POM in Chukchi Shelf

The properties of water samples collected from different depths and locations reveal major contrasts in the compositions of suspended particles throughout the Chukchi Shelf during the late, open-water season. One way to evaluate such contrast is illustrated in plots of POC vs. Chl Fl for samples collected during the two cruises (Fig. 17). Among the trends evident in these graphs, we highlight samples from low- to intermediate-density waters ($_{t}$ < 26 kg m^{-3}) that exhibit high Chl Fl:POC ratios (> 10 mg g^{-1}) consistent with actively growing phytoplankton (e.g. Geider, 1987; Sathyendranath et al., 2020). In both cruises, the highest Chl:POC ratios (> 20 mg g^{-1}) are from samples within a narrower density range (25 < $_{t}$ < 26 kg m^{-3}) from both BCSW and BCWW associated with pycnocline depths. These high pigment-to-carbon ratios likely reflect low-light acclimated phytoplankton that are most abundant at the depths associated with the SCM. Exceptions to these trend include some of the intermediate-density (23 < $_{t}$ < 24.5 kg m^{-3}) samples collected during SKQ201712S, and especially those collected following the upwelling wind event, which are characterized by relatively low Chl Fl:POC ratios (5 to 10 mg g^{-1}; Fig. 17c and d). These samples correspond to warm BCSW and ACW samples from the surface, which have moderately elevated photosynthetic pigment concentrations (Table 3) and suggest the presence of phytoplankton acclimated to higher light intensities at these locations. The other major type of particles evident from this plot are samples from high-density ($_{t}$ > 25.5 kg m^{-3}) bottom waters that are characterized by low Chl Fl:POC (5 mg g^{-1}) ratios (Fig. 17), which are characterized by low overall chlorophyll concentrations and elevated c_p signals (Tables 2 and 3). As described below these compositions suggest significant contributions of mineral-rich particles that originate from the seabed.

Plots of c_p vs. POC data for various density ranges (Figure 18) provide additional evidence for the presence of different particle pools throughout the water column of the NE Chukchi Shelf during the late, open-water season. The graphs for both SKQ201612S and SKQ201712S prior and after wind events highlight the stark contrasts between samples collected from high-density ($_{t}$

> 25.5 kg m^{-3}) bottom waters (both BCSW and BCWW), and samples from low- to intermediate-density ranges characteristic of surface and mid-depth waters (MW, ACW and BCSW). These latter samples are characterized by elevated POC:c_p ratios ~ 30 mmol m^{-2}, that are consistent with the global POC-beam attenuation relationships determined by Gardner and co-workers (2006) for plankton-dominated open ocean particles. In contrast, the markedly lower POC:c_p ratios ($<$ 10 mmol m^{-2}) of high-density BCSW and BCWW indicate the high turbidity of the waters below the pycnocline contain particles with high mass-specific scattering coefficients that would be expected from mineral-rich detrital materials (e.g., Goñi et al., 2021; Gardner et al., 2001). These low POC:c_p ratios are consistent with contributions from sediment sources either through local resuspension from the seabed and/or lateral advection from up-stream regions. The fact that this particle pool is ubiquitous in both BCSW and BCWW bottom waters throughout the North East Chukchi shelf during both cruises is consistent with relatively high energy due to currents and/or waves in order to sustain these high levels of particle resuspension.

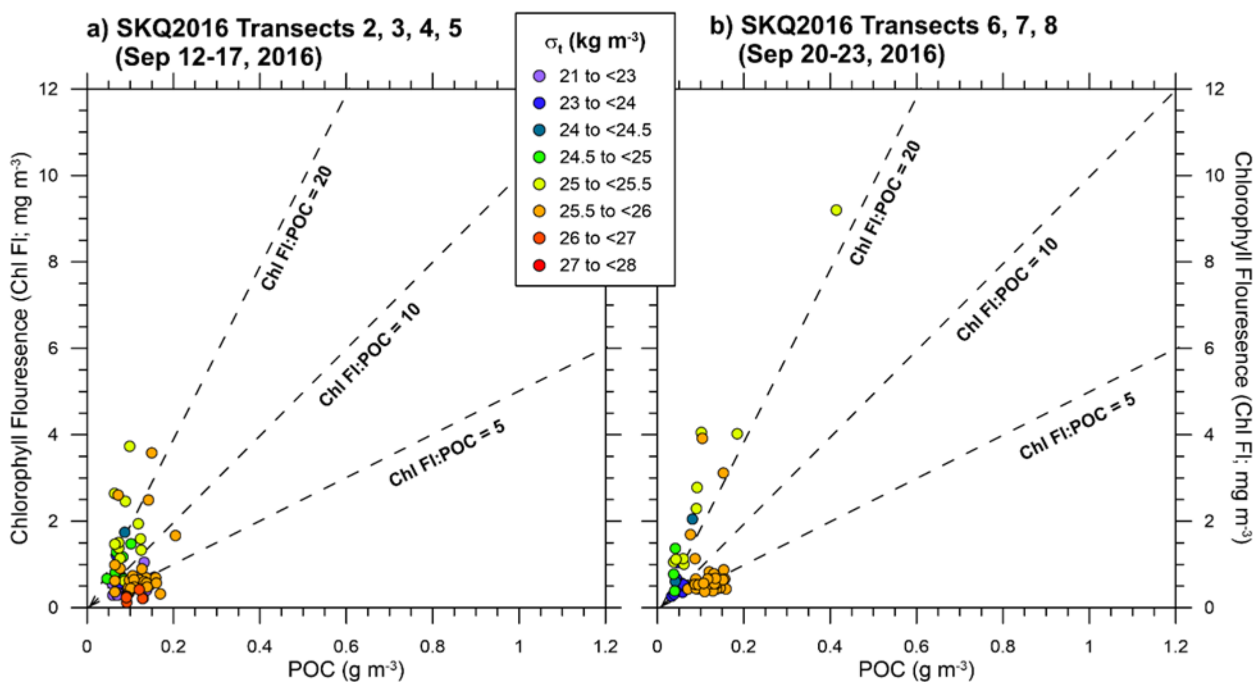

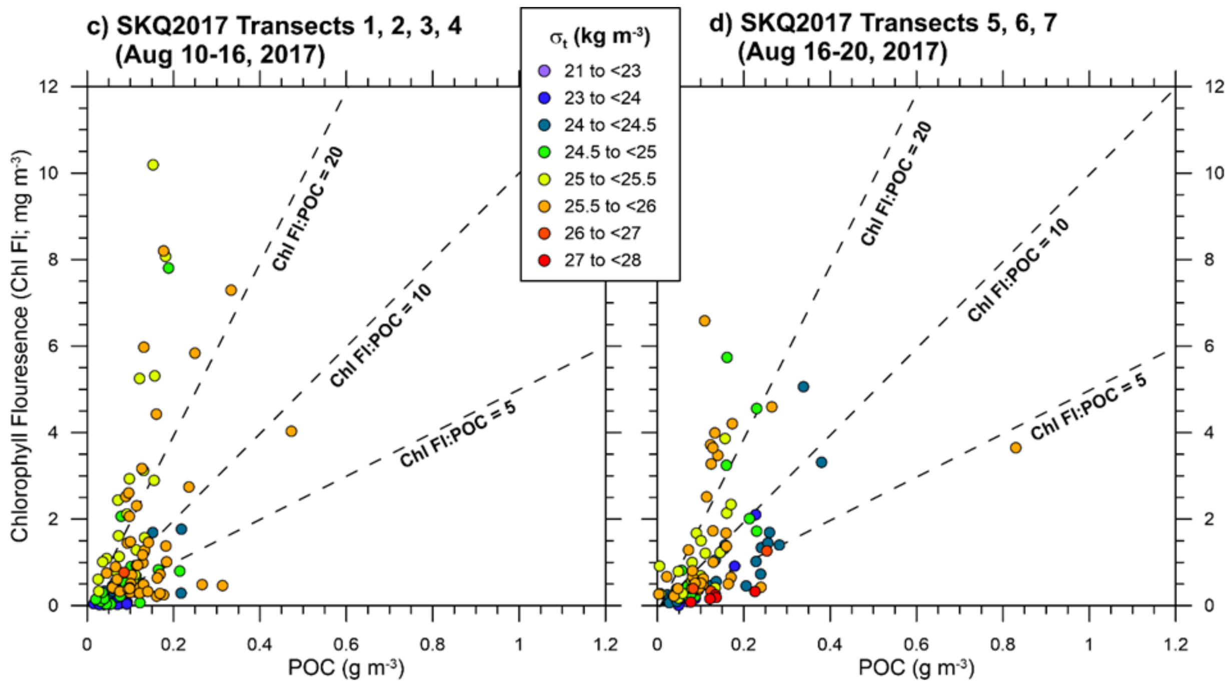

Figure 17. Plots of particulate organic carbon (POC; g m^{-3}) concentrations vs. chlorophyll fluorescence (Chl Fl; mg m^{-3}) sensor data for individual water samples from stations occupied during SKQ201612S before and after the Sep 17-20, 2016 downwelling-favorable wind event (a and b, respectively) and during SKQ201712S before and after the August 12-17, 2017 upwelling-favorable wind (c and d, respectively). Data are shown in different colors according to their density ranges (e.g. see Tables 2 and 3). Included in each graph are lines illustrating different Chl Fl:POC ratios (mg g^{-1}) for reference.

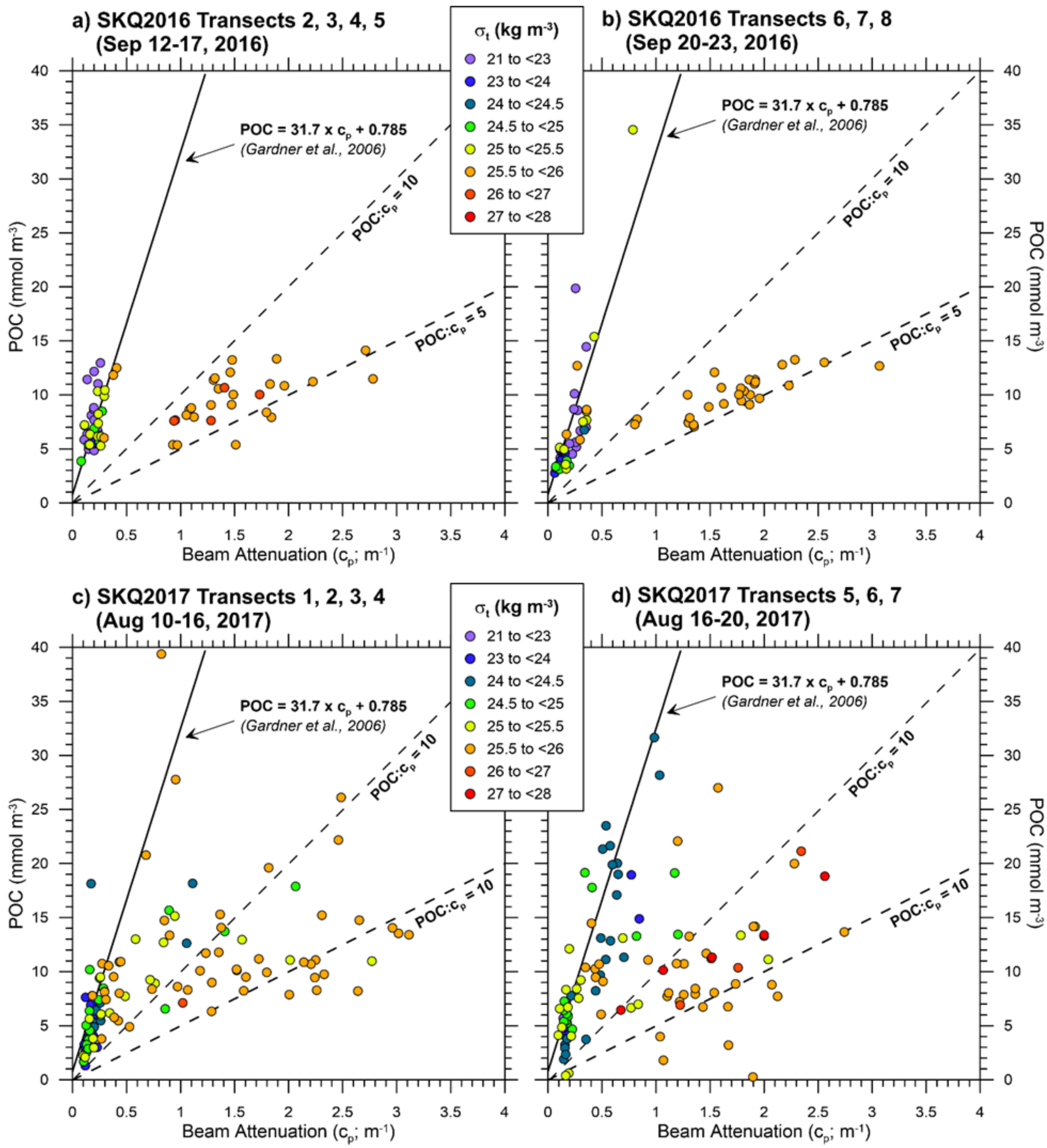

Figure 18. Plots of particulate beam attenuation sensor data (c_p; m^{-1}) vs. particulate organic carbon (POC; mmol m^{-3}) concentrations for individual water

samples from stations occupied during SKQ201612S before and after the Sep 17-20, 2016 downwelling-favorable wind event (a and b, respectively) and during SKQ201712S before and after the August 12-17, 2017 upwelling-favorable wind (c and d, respectively). Data are shown in different colors according to their density ranges (e.g. see Tables 2 and 3). Included in each graph are lines illustrating different POC:c_p ratios (mmol m^{-2}) for reference, including the global average relationship measured by Gardner et al., 2006.

Table 4 summarizes the Chl Fl:POC and POC:cp ratios of the different density ranges for the various water masses encountered during SKQ201612S and SKQ201712S and includes other parameters that help elucidate the composition and provenance of POM in samples from the NE Chukchi Shelf during late open-water season. For example, because pheophytin is a decay product of chlorophyll (e.g., Bianchi et al., 1988; Strom 1993), we can examine the relative abundances of these two pigments to evaluate the freshness (and viability) of phytoplankton derived organic matter in our POM samples. Previous studies from the Chukchi Sea (McTigue et al., 2015) showed that surface sediments from sites across the shelf that received fresh input of phytoplankton exhibited low Pheo/(Chl+Pheo) (< 0.2) ratios whereas locations where degradation by microbial and herbivorous grazing was more significant displayed higher Pheo/(Chl+Pheo) ratios (> 0.2). Although our suspended POM pigment analyses are somewhat sparse, the distributions of Pheo/(Chl+Pheo) ratios tabulated in Table 4 clearly show that during both SKQ201612S and SKQ201712S, the vast majority of low- and intermediate-density ($_t$ < than 25.5 kg m^{-3}) water masses throughout the top half of the water column across the Chukchi Shelf are characterized by pigment compositions indicative of relative fresh phytoplankton sources. In contrast, the high-density ($_t$ > 25.5 kg m^{-3}) water masses that occupy the lower half of the water column across the Chukchi Shelf during both cruises, and which correspond to BCSW and BCWW, are characterized by significantly elevated Pheo/(Chl+Pheo) ratios consistent with contributions from degraded phytodetritus. The main exception to this trend are samples from high-density BCSW collected during SKQ201712S after the upwelling wind event (Table 3). These samples display low Pheo/(Chl+Pheo) ratios that suggest inputs from fresh phytoplankton (Table 4).

Another parameter that displays trends consistent with distinct particle compositions is the POC:SPM ratio (Table 4), which similarly to the trends in POC:c_p ratios discussed above, tends to be higher (4 %) in samples from low- to intermediate-density waters and is lower (1 to 2 %) in high-density waters. The observed ranges in POC:SPM ratios (Table 4) are comparable to the compositional data from samples collected over a full season in 2016 by a bottom-moored sediment trap located at site offshore Wainwright (Chukchi Ecosystem Observatory; Lalande et al., 2020) that coincides with our transect locations (Fig. 1). The materials collected in the sediment trap were characterized by Chl:POC ratios that ranged from < 0.5 mg g^{-1} during the winter months, to ~ 5 mg g^{-1} in the early open water season (June and July). In addition, these same samples exhibited POC:SPM mass ratios that ranged from 2% in the winter to $> 4\%$ in the mid-summer periods of high productivity (data from Lalande et al., 2020). Notably, data from the ICESCAPE project in June-July of 2011 (Neukermans et al., 2014) showed that samples from surface waters exhibiting under-ice phytoplankton blooms showed lower Chl:POC ratios (10 mg g^{-1}) and much higher POC:SPM (40%) ratios than those collected from the SCM regions during the two late-season open water cruises. In contrast, the compositions of samples from bottom waters with high turbidity collected during ICESCAPE displayed moderate Chl:POC (4 mg g^{-1}) and POC:SPM (1.4%) ratios that were similar to the ones collected from high density BCSW and BCWW in this study. Thus, it appears that the particles present in the water column of the northeast Chukchi Shelf during the late summer display compositions that are consistent with a heterogeneous mixture of POM sources that are distinct from those present during the early summer.

6 Summary and Future Work

The hydrographic characteristics across the water column of the Northeast Chukchi Sea during the late summer are consistent with previous studies (e.g., Danielson et al., 2017; Weingartner et al., 2017) and show the highly stratified water column has a fundamental impact on the distribution and composition of POM in the region. Contrasts in POM compositional ratios (e.g., Chl:POC, POC:SPM, POC:c_p) indicate the presence of different types of particles in distinct regions and depths of the study area, including the nutrient depleted surface layers, the mid-depths with characteristic SCM, and the highly turbid deeper waters. We conclude that the spatial and temporal contrasts in water mass distributions and the impacts of distinct wind forcings lead to different biogeochemical responses. For example, changes consistent with enhanced phytoplankton production (increases in Chl and POC) occur in surface waters across Barrow Canyon and in nearshore regions associated with ACW in response to upwelling. Furthermore, similar biological responses are also observed in mid-depth regions of the water column at the interface between MW and BCWW around Hannah Shoal in response to downwelling-favorable winds. The large temporal and spatial variability in particulate compositions illustrates the highly dynamic nature of POM in the northeast Chukchi Shelf and reflects the complex productivity and provenance regimes that characterize this region of the Arctic Ocean. Our results suggest the extent of phytoplankton productivity in the surface and subsurface regions of the Chukchi Sea during the late open-water season varies as a function of water mass distributions, wind forcing, and location relative to bathymetric and topographic features such as canyons, shoals and capes.

Work to evaluate other biogeochemical tracers of primary productivity, including dissolved oxygen and nutrients, across the Northeast Chukchi Sea during the open water season is on-going. Examination of the distribution and dynamics of these productivity tracers along with incubation-based measurements of primary production will help us further understand the controls on the biological response to climate change of this and other Arctic marginal seas and start addressing the underlying mechanisms that may be responsible for the 'greening' of the Arctic Ocean (e.g., Ardyna and Arrigo, 2020). To fully evaluate the impacts of climate change on Arctic ocean ecology and biogeochemistry, future studies should focus on enhancing the spatial and temporal coverage across complex hydrographic regions such as the Chukchi Sea throughout the polar seasons.

Acknowledgments, Samples, and Data

We thank the captains and crew of the R/V Sikuliaq who facilitated the completion of this work during the two cruises. Emmanuel Alegria, Sydney Clark, Elizabeth Corvi, Kimberly Craig, Erin Guillory and Quinn Roberts provided valuable help in the collection and analyses of water samples. The science crews of SKQ201612S and SKQ201712S were critical in helping complete the CTD surveys during both cruises.

All the data, including CTD profiles and individual sample compositions from Niskin bottles are archived in the Arctic Data Center (pending doi's; in the meantime, see supplement Tables 1S and 2S). All the CTD profile data are available at the Rolling Deck to Repository (R2R) data repository for R/V Sikuliaq's cruises SKQ201612S and SKQ210712S (https://www.rvdata.us/search/cruise/SKQ201612S12S and https://www.rvdata.us/search/cruise/SKQ201712S12S, respectively.

All remaining filter samples are stored in M. Goñi's laboratory.

References

Allen, M.R., Dube, O.P., Solecki, W., Aragón-Durand, F., Cramer, W., Humphreys, S., Kainuma, M., Kala, J., Mahowald, N., Mulugetta, Y., Perez, R., Wairiu, M., Zickfeld, K. (2018) Framing and Context. In: Global Warming of 1.5°C. An IPCC Special Report on the impacts of global warming of 1.5°C above pre-industrial levels and related global greenhouse gas emission pathways, in the context of strengthening the global response to the threat of climate change, sustainable development, and efforts to eradicate poverty [Masson-Delmotte, V., P. Zhai, H.-O. Pörtner, D. Roberts, J. Skea, P.R. Shukla, A. Pirani, W. Moufouma-Okia, C. Péan, R. Pidcock, S. Connors, J.B.R. Matthews, Y. Chen, X. Zhou, M.I. Gomis, E. Lonnoy, T. Maycock, M. Tignor, and T. Waterfield (eds.)]. In Press.Arar, E., and Collins, G.B. (1997). Method 445.0 In Vitro Determination of Chlorophyll a and Pheophytin in Marine and Freshwater Algae by Fluorescence. Washington, DC.

Arar, E. J., Collins, G.B. (1997) Method 445.0 In Vitro Determination of Chlorophyll a and Pheophytin ain Marine and Freshwater Algae by Fluorescence. U.S. Environmental Protection Agency, Washington, DC, Revision 1.2, pp. 22.

Ardyna, M., and Arrigo, K.R. (2020). Phytoplankton dynamics in a changing Arctic Ocean. Nature Climate Change 10, 892-903.

Ardyna, M., Babin, M., Gosselin, M., Devred, E., Belanger, S., Matsuoka, A., Tremblay, J.-E. (2013). Parameterization of vertical chlorophyll a in the Arctic

Ocean: impact of the subsurface chlorophyll maximum on regional, seasonal, and annual primary production estimates. Biogeosciences, 10, 4383–4404, 2013.

Ardyna, M., Mundy, C.J., Mills, M.M., Oziel, L., Grondin, P.-L., Lacour, L., Verin, G., van Dijken, G., Ras, J., Alou-Font, E., Babin, M., Gosselin, M., Tremblay, J.-E., Raimbault, P., Assmy, P., Nicolaus, M, Claustre, H., Arrigo, K.R. (2020). Environmental drivers of under-ice phytoplankton bloom dynamics in the Arctic Ocean. Elem. Sci. Anth., 8:30, doi.org/10.1525/elementa.430.

Arrigo, K.R. and van Dijken, G.L. (2015). Continued increases in Arctic Ocean primary production. Progress in Oceanography 136, 60-70.

Arrigo, K.R., Perovich, D.K., Pickart, R.S., Brown, Z.W., van Dijken, G.L., Lowry, K.E., Mills, M.M., Palmer, M.A., Balch, W.M., Bahr, F., Bates, N.R., Benitez-Nelson, C., Bowler, B., Brownlee, E., Ehn, J.K., Frey, K.E., Garley, R., Laney, S.R., Lubelczyk, L., Mathis, J., Matsuoka, A., Mitchell, B.G., Moore, G.W.K., Ortega-Retuerta, E., Pal, S., Polashenski, C.M., Reynolds, R.A., Scheiber, B., Sosik, H.M., Stephens, M., Swift, J.H. (2012). Massive phytoplankton blooms under Arctic sea ice. Science 336, 1408.

Arrigo, K.R., Perovich, D.K., Pickart, R.S., Brown, Z.W., van Dijken, G.L., Lowry, K.E., Mills, M.M., Palmer, M.A., Balch, W.M., Bates, N.R., Benitez-Nelson, C.R., Brownlee, E., Frey, K.E., Laney, S.R., Mathis, J., Matsuoka, A., Mitchell, B.G., Moore, G.W.K., Reynolds, R.A., Sosik, H.M., Swift, J.H. (2014). Phytoplankton blooms beneath the sea ice in the Chukchi Sea. Deep Sea Research Part II 105, 1–16. http://dx.doi.org/10.1016/j.dsr2.2014.03.018Arrigo et al., 2013

Bates, N.R., Hansell, D.A., Moran, S.B., Codispoti, L.A. (2005). Seasonal and spatial distribution of particulate organic matter (POM) in the Chukchi and Beaufort Seas. Deep-Sea Research II 52 (2005) 3324–3343.

Bianchi, T.S., Dawson, R., Sawangwong, P. (1988). The effects of macrobenthic deposit-feeding on the degradation of chloropigments in sandy sediments. J Exp Mar Biol Ecol 122: 243–255. doi:10.1016/0022-0981(88)90126-8.

Bröder, L., Andersson, A., Tesi, T., Semiletov, I., & Gustafsson, Ö. (2019). Quantifying degradative loss of terrigenous organic carbon in surface sediments across the Laptev and East Siberian Sea. Global Biogeochemical Cycles, 33, 85–99. https://doi.org/10.1029/2018GB005967.

Brown, Z.W., Lowry, K.E., Palmer, M.A., van Dijken, G.L., Mills, M.M., Pickart, R.S., Arrigo, K.R. (2015). Characterizing the subsurface chlorophyll a maximum in the Chukchi Sea and Canada Basin. Deep-Sea ResearchII118(2015)88–104.

Chaves, J.E., Cetinić, I., Dall'Olmo, G., Estapa, M., Gardner, W., Goñi, M., Graff, J.R., Hernes, P., Lam, P.J., Liu, Z., Lomas, M.W., Mannino, A., Novak, M.G., Turnewitsch, R., Werdell, P.J., Westberry, T.K., (2021) Particulate

Organic Matter Sampling and Measurement Protocols: Consensus Towards Future Ocean Color Missions. NASA Ocean Ecology Lab Field Support Group and hosted at NASA Goddard Space Flight Center in Nov. 30- Dec 2, 2016.

Coachman, L.K., Aagaard, K., Tripp, R.B., 1975. Bering Strait: the Regional Physical Oceanography. University of Washington Press, Seattle, WA (172pp).

Danielson, S.L., Weingartner, T.J., Hedstrom, K.S., Aagaard, K., Woodgate, R., Curchitser, E., Stabeno, P.J. (2014). Coupled wind-forced controls of the Bering-Chukchi shelf circulation and the Bering Strait throughflow: Ekman transport, continental shelf waves, and variations of the Pacific–Arctic sea surface height gradient. Prog.Oceanogr.125,40–61. http://dx.doi.org/10.1016/j.pocean.2014.04.006.

Danielson, S.L., Eisner, L., Ladd, C., Mordy, C., Sousa, L., Weingartner, T.J. (2017) A comparison between late summer 2012 and 2013 water masses, macronutrients, and phytoplankton standing crops in the northern Bering and Chukchi Seas. Deep-Sea Research II, 135, 7-26.

Danielson, S., Hedstrom, K., Hennon, T., Mordy, C., Stabeno, P., Stockwell, D., Woodgate, R. (2021) Recent Volume, Heat, and Nutrient Fluxes on the Pacific Arctic Continental Shelf. Abstract in 2021 Alaskan Marine Science Symposium, p.160.

Fetterer, F., Knowles, K., Meier, W., Savoie, M., Windnagel, A.K. (2017). Sea Ice Index, Version 3. Sea Ice Extent and Concentration. NSIDC: National Snow and Ice Data Center, Boulder, Colorado USA. https://doi.org/10.7265/N5K072F8. updated daily. (September 5, 2018).

Forest, A., Sampei, M., Hattori, H., Makabe, R., Sasaki, H., Fukuchi, M., Wassmann, P., Fortier, L. (2007). Particulate organic carbon fluxes on the slope of the Mackenzie Shelf (Beaufort Sea): Physical and biological forcing of shelf-basin exchanges. Journal of Marine Systems 68 (2007) 39–54.

Forest, A., Babin, M., Stemmann, L., Picheral, M., Sampei, M., Fortier, L., Gratton, Y., Belanger, S., Devred, E., Sahlin, J., Doxaran, D., Ortega-Retuerta, E., Martin, J., Jeffrey, W.H., Gasser, B., Carlos Miquel, J. (2013). Ecosystem function and particle flux dynamics across the Mackenzie Shelf (Beaufort Sea, Arctic Ocean): an integrative analysis of spatial variability and biophysical forcings. Biogeosciences, 10, 2833–2866.

Forest, A., Osborne, P.D., Fortier, L., Sampei, M., Lowings, M.G. (2015). Physical forcings and intense shelf–slope fluxes of particulate matter in the halocline waters of the Canadian Beaufort Sea during winter. Continental Shelf Research, 101, 1-21.

Foukal, N. P., Pickart, R. S., Moore, G.W. K., & Lin, P. (2019). Shelf break downwelling in the Alaskan Beaufort Sea. Journal of Geophysical Research: Oceans, 124, 7201 7225. https://doi.org/10.1029/2019JC015520

Gardner, W.D., Blakey, J.C., Walsh, I.D., Richardson, M.J., Pegau, S., Zaneveld, J.R.V., Roesler, C., Gregg, M.C., MacKinnon, J.A., Sosik, H.M., Williams, A.J. (2001). Optics, particles, stratification, and storms on the New England continental shelf. Journal of Geophysical Research—Oceans, 106, 9473–9497.

Gardner, W.D., Mishonov, A.V., Richardson, M.J. (2006). Global POC concentrations from in-situ and satellite data. Deep-Sea Research II, 53, 718–740.

Geider, R.J. (1987). Light and temperature dependence of the carbon to chlorophyll a ratio in microalgae and cyanobacteria: implications for physiology and growth of phytoplankton. New Phytologist 106, 1–34.

Goñi, M.A., Corvi, E.R., Welch, K.A., Buktenica, M., Lebon, K., Alleau, Y., Juranek L.W. (2019). Particulate organic matter distributions in surface waters of the Pacific Arctic shelf during the late summer and fall season. Marine Chemistry, https://doi.org/10.1016/j.marchem.2019.03.010.

Goñi, M.A., Corvi, E.R., Welch, K.A., Alegria, E., Watkins-Brandt, K., White A.E. (2021) Wintertime particulate organic matter distributions in surface waters of the northern California current system. Continental Shelf Research, 213, https://doi.org/10.1016/j.csr.2020.104312.

Grebmeier, J. M., Bluhm, B. A., Cooper, L. W., Danielson, S. L., Arrigo, K. R., Blanchard, A. L., et al. (2015). Ecosystem characteristics and processes facilitating persistent macrobenthic biomass hotspots and associated benthivory in the Pacific Arctic. Progress in Oceanography, 136, 92–114. https://doi.org/10.1016/j.pocean.2015.05.006.

Grebmeier, J.M., Moore, S.E., Cooper, L.W., Frey, K.E. (2019) The Distributed Biological Observatory: A change detection array in the Pacific Arctic – An introduction. Deep-Sea Research Part II 162 (2019) 1–7. https://doi.org/10.1016/j.dsr2.2019.05.005.

Hill, V., and Cota, G. (2005). Spatial patterns of primary production on the shelf, slope and basin of the Western Arctic in 2002. Deep Sea Research Part II: Topical Studies in Oceanography, 52(24–26), 3344–3354. https://doi.org/10.1016/j.dsr2.2005.10.001.

Huntington, H.P., Danielson, S.L., Wiese, F.K., Baker, M., Boveng, P., Citta, J.J., De Robertis, A., Dickson, D.M.S., Farley, E., Craighead George, J., Iken, K., Kimmel, D.G., Kuletz, K., Ladd, C., Levine, R., Quakenbush, L., Stabeno, P., Staffortd, K.M., Stockwell, D., Wilson, C. (2020). Evidence suggests potential transformation of the Pacific Arctic ecosystem is underway. Nature Climate Change, 10, 342-348, https://doi.org/10.1038/s41558-020-0695-2.

Jackson, J.M., Allen, S.E., McLaughlin, F.A., Woodgate, R.A., Carmack, E.C., (2011). Changes to the near-surface waters in the Canada Basin, Arctic Ocean from 1993–2009: a basin in transition. J. Geophys. Res. 116 (C10), C10008.

Juranek, L., Takahashi, T., Mathis, J., and Pickart, R. (2019). Significant biologically mediated CO2 uptake in the Pacific Arctic during the late open water season. Journal of Geophysical Research: Oceans, 124, 821–843. https://doi.org/10.1029/2018JC014568.

Konar, B., Frisch, L., Moran, S.B. (2017). Development of best practices for scientific research vessel operations in a changing Arctic: A case study for R/V Sikuliaq. Marine Policy 86 (2017) 182–189.

Lalande, C., Grebmeier, J.M., Hopcroft, R.R., Danielson, S.L. (2020) Annual cycle of export fluxes of biogenic matter near Hanna Shoal in the northeast Chukchi Sea. Deep Sea Research II, 177, https://doi.org/10.1016/j.dsr2.2020.104730.

Lewis, K.M., van Dijken, G.L., Arrigo, K.R. (2020). Changes in phytoplankton concentration now drive increased Arctic Ocean primary production. Science 369, 198–202.

Lin, P., Pickart, R. S., Moore, G. W. K., Spall, M. A., & Hu, J. (2019). Characteristics and dynamics of wind-driven upwelling in the Alaskan Beaufort Sea based on six years of mooring data. Deep-Sea Research Part II: Topical Studies in Oceanography, 162, 79–92. https://doi.org/10.1016/j.dsr2.2018.01.002.

Lowry, K., Pickart, R., Mills, M., Brown, Z., van Dijken, G., Bates, N., Arrigo, K. (2015). Influence of winter water on phytoplankton blooms in the Chukchi Sea. Deep Sea Res. II 118, 53–72.

Martini, K. I., P. J. Stabeno, C. Ladd, P. Winsor, T. J. Weingartner, C. W. Mordy, Eisner, L. B. (2016). Dependence of subsurface chlorophyll on seasonal water masses in the Chukchi Sea, J. Geophys. Res. Oceans, 121, 1755–1770, doi:10.1002/2015JC011359.

McLaughlin, F. A., and Carmack, E. C. (2010). Deepening of the nutricline and chlorophyll maximum in the Canada Basin interior, 2003–2009, Geophys. Res. Lett., 37, L24602, doi:10.1029/2010GL045459.

McTigue, N.D., Bucolo, P., Liu, Z., Dunton, K.H. (2015). Pelagic-benthic coupling, food webs, and organic matter degradation in the Chukchi Sea: Insights from sedimentary pigments and stable carbon isotopes. Limnol. Oceanogr. 60, 2015, 429–445; doi: 10.1002/lno.10038

Moran, S.B., Kelly, R.P., Hagstrom, K., Smith, J.N., Grebmeier, J.M., Cooper, L.W., Cota, G.F., Walsh, J.J., Bates, N.R., Hansell, D.A., Maslowski, W., Nelson, R.P., Mulsow, S. (2005). Seasonal changes in POC export flux in the Chukchi Sea and implications for water column-benthic coupling in Arctic shelves. Deep-Sea Research II, 52, 3427–3451.

Neukermans, G., R. A. Reynolds, Stramski. D. (2014). Contrasting inherent optical properties and particle characteristics between an under-ice phytoplankton bloom and open water in the Chukchi Sea. Deep Sea Res., Part II, 105, 59–73. doi:10.1016/j.dsr2.2014.03.014.

Neukermans, G., Reynolds, R.A., Stramski, D. (2016). Optical classification and characterization of marine particle assemblages within the western Arctic Ocean. Limnol. Oceanogr. 61, 2016, 1472–1494.

Nguyen, A. T., Woodgate, R. A., Heimbach, P. (2020). Elucidating large-scale atmospheric controls on Bering Strait throughflow variability using a data-constrained ocean model and its adjoint. Journal of Geophysical Research: Oceans, 125, e2020JC016213. https://doi.org/10.1029/2020JC016213

Nishino, S., Kawaguchi, Y., Inoue, J., Yamamoto-Kawai, M., Aoyama, M., Harada, N., Kikuchi, T. (2020). Do strong winds impact water mass, nutrient, and phytoplankton distributions in the ice-free Canada Basin in the fall?. Journal of Geophysical Research: Oceans, 125, e2019JC015428. https://doi.org/10.1029/2019JC015428.

Okkonen, S., Ashjian, C., Campbell, R.G., Alatalo, P. (2019) The encoding of wind forcing into the Pacific-Arctic pressure head, Chukchi Sea ice retreat and late-summer Barrow Canyon water masses. Deep-Sea Research Part II 162 (2019) 22–31. https://doi.org/10.1016/j.dsr2.2018.05.009.

Pacini, A., Moore, G. W. K., Pickart, R. S., Nobre, C., Bahr, F., Våge, K., Arrigo, K. R. (2019). Characteristics and transformation of Pacific winter water on the Chukchi Sea shelf in late-spring. Journal of Geophysical Research: Oceans, 124, 7153 7177. https://doi.org/10.1029/2019JC015261.

Parsons, T.R., Y. Maita, and C.M. Lalli. 1984. A Manual of Chemical & Biological Methods for Seawater Analysis. Elsevier. https://linkinghub.elsevier.com/retrieve/pii/C20090077745

Pickart, R. S., Schulze, L. M., Moore, G. W. K., Charette, M. A., Arrigo, K. R., van Dijken, G., & Danielson, S. L. (2013). Long-term trends of upwelling and impacts on primary productivity in the Alaskan Beaufort Sea. Deep-Sea Research Part I: Oceanographic Research Papers,79, 106–121. https://doi.org/10.1016/j.dsr.2013.05.003.

Pickart, R. S., Nobre, C., Lin, P., Arrigo, K. R., Ashjian, C. J., Berchok, C., Cooper, L.W., Grebmeier, J.M., Hartwell, I., He, J., Itoh, M., Kikuchi, T., Nishino, S., Vagle, S. (2019). Seasonal to mesoscale variability of water masses and atmospheric conditions in Barrow Canyon, Chukchi Sea. Deep-Sea Research Part II: Topical Studies in Oceanography, 162, 32–49. https://doi.org/10.1016/j.dsr2.2019.02.003.

Pisareva, M.N., Pickart, R.S., Lin, P., Fratantoni, P.S., Weingartner, T.J., (2019). On the nature of wind-forced upwelling in Barrow Canyon. Deep-Sea Research Part II 162 (2019) 63–78. https://doi.org/10.1016/j.dsr2.2019.02.002.

Reynolds R.A. and Stramski, D. (2019) Optical characterization of marine phytoplankton assemblages within surface waters of the western Arctic Ocean. Limnol. Oceanogr. 64, 2019, 2478–2496, doi: 10.1002/lno.11199.

Sathyendranath, S., Platt, T., Kovac, Z., Dingle, J. Jackson, T., Brewin, R.J.W., Franks, P., Marañon, E., Kulk, G., Bouman, H.A. (2020). Reconciling models of primary production and photoacclimation. Applied Optics 59, https://doi.org/10.1364/AO.386252.

Shroyer, E.L., and Pickart, R.S. (2019). Pathways, timing, and evolution of Pacific Winter Water through Barrow Canyon. Deep-Sea Research Part II, 162, 50–62.

Slagstad, D., Wassmann, P.F.J. Ellingsen, I. (2015). Physical constrains and productivity in the future Arctic Ocean. Front. Mar. Sci., 2:85, doi: 10.3389/fmars.2015.00085.

Stabeno, P.J., Mordy, C.W., Sigler, M.F. (2020). Seasonal patterns of near-bottom chlorophyll fluorescence in the eastern Chukchi Sea: 2010–2019. Deep-Sea Research Part II, 177, 104842. https://doi.org/10.1016/j.dsr2.2020.104842.

Stavn, R.H., Rick, H.J., Falster, A.V. (2009). Correcting the errors from variable sea salt retention and water of hydration in loss on ignition analysis: Implications for studies of estuarine and coastal waters. Estuarine, Coastal and Shelf Science, 81, 575–582.

Stramski, D., Babin, M., Wozniak, S.B. (2007). Variations in the optical properties of terrigenous mineral-rich particulate matter suspended in seawater. Limnol. Oceanogr., 52(6), 2418–2433.

Stroeve, J., and Notz, D. (2018). Changing state of Arctic sea ice across all seasons. Environ. Res. Lett.13 103001, doi: 10.1088/1748-9326/aade56.

Strom, S. L. (1993). Production of pheopigments by marine protozoa—results of laboratory experiments analyzed by HPLC. Deep-Sea Res I 40: 57–80. doi:10.1016/0967-0637(93)90053-6.

Vonk, J.E., Tank, S.E., Bowden, W.B., Laurion, I., Vincent, W.F., Alekseychik, P., Amyot, M., Biller, M.F., Canario, J., Cory, R.M., Deshpande, B.N., Helbig, M., Jammet, M., Karlsson, J., Larouche, J., MacMillan, G., Rautio, M, Walter Anthony, K.M., Wickland, K.P. (2015). Reviews and syntheses: Effects of permafrost thaw on Arctic aquatic ecosystems. Biogeosciences, 12, 7129–7167, doi:10.5194/bg-12-7129-2015.

Weingartner, T., Aagaard, K., Woodgate, K., Danielson, R., Sasaki, S., Cavalieri, D, Y. (2005). Circulation on the north central Chukchi Sea shelf. Deep-Sea Res. Part II, 52, 3150–3174.

Weingartner, T., Fang, Y.-C., Winsor, P., Dobbins, E., Potter, R., Statscewich, H., Mudge, T., Irving, B., Sousa, L., Borg, K. (2017). The summer hydrographic structure of the Hanna Shoal region on the northeastern Chukchi Sea shelf: 2011–2013. Deep-Sea Research Part II, 144, 6–20.

Wood, K.R., Bond, N.A., Danielson, S.L., Overland, J.E., Salo, S.A., Stabeno, P.J., Whitefield, J. (2015). A decade of environmental change in the Pacific

Arctic region. Progress in Oceanography, 136, 12–31. http://dx.doi.org/10.1016/j.pocean.2015.05.005.

Woodgate, R.A., Stafford, K.M., Prahl, F.G. (2015). A synthesis of year-round interdisciplinary mooring measurements in the Bering Strait (1990–2014) and the RUSALCA years (2004–2011). Oceanography 28(3):46–67, http://dx.doi.org/10.5670/oceanog.2015.57.

Woodgate, R.A. (2018). Increases in the Pacific inflow to the Arctic from 1990 to 2015, and insights into seasonal trends and driving mechanisms from year-round Bering Strait mooring data. Progress in Oceanography 160, 124–154, https://doi.org/10.1016/j.pocean.2017.12.007.

Yamamoto-Kawai, M., McLaughlin, F.A., Carmack, E.C., Nishino, S., Shimada, K., Kurita, N. (2009). Surface freshening of the Canada Basin, 2003–2007: river runoff versus sea ice meltwater. J. Geophys. Res. Oceans 114.

Zhang, J., Spitz, Y.H., Steele, M., Ashjian, C., Campbell, R., Berline, L., Matrai, P. (2010). Modeling the impact of declining sea ice on the Arctic marine planktonic ecosystem, J. Geophys. Res., 115, C10015, doi:10.1029/2009JC005387.